

**NET ECOSYSTEM METABOLISM IN THE LOWER COLUMBIA AND
WILLAMETTE RIVERS**

by
Nikolai M. Danilchik

A THESIS

Presented to the Division of Environmental & Biomolecular Systems
and the Oregon Health & Science University
School of Medicine
in partial fulfillment of the requirements for the degree of

Master of Science
in
Environmental Science and Engineering

September 2018

School of Medicine
Oregon Health & Science University

Certificate of Approval

This is to certify that the Master's Thesis of

Nikolai M. Danilchik

*“Net Ecosystem Metabolism in the Lower Columbia and
Willamette Rivers”*

Has been approved



Thesis Advisor



Committee Member



Committee Member

Table of Contents

Certificate of Approval	ii
Table of Contents	iii
List of Figures	v
List of Tables	vi
Acknowledgements.....	vii
Abstract.....	ix
Chapter 1: Introduction	1
1.0 Overview of the Columbia River System	1
1.1 Hydrography	1
1.2 Hydroelectric Dams and the Greening of the Columbia.....	3
2.0 Aquatic Primary Production.....	5
2.1 General Principles.....	5
2.2 The Mixing Question	8
3.0 Measuring Aquatic Primary Production in Rivers	10
3.1 BOD “Light/Dark” Incubation Method	10
3.2 Sensor-Based Open Water Method.....	12
3.3 Chlorophyll	17
3.4 Inorganic Nutrients	19
3.5 Photosynthetically Active Radiation.....	20
4.0 Study Rationale and Objectives	23
5.0 References	24
Chapter 2: Primary Production and Vertical Mixing in the Columbia and Willamette Rivers.....	29
1.0 Abstract.....	29
2.0 Introduction.....	30
3.0 Materials and Methods.....	32
3.1 Sensor-Based Calculations.....	32
3.1.1 CMOP Campaign and Site Description	32
3.1.2 Protocol.....	33
3.2 Sampling-Based Calculations	34
3.2.1 Sampling Protocol.....	34
3.2.2 BOD Bottle Incubations.....	34
3.2.3 Chlorophyll	37

3.2.4 Inorganic Nutrients	38
3.3 Field Measurements	38
3.3.1 CTD Casts and Light Attenuation.....	38
3.3.2 Water Column Stratification	39
4.0 Results	40
4.1 GPP and ER	40
4.2 Chlorophyll and particulate organic carbon.....	46
4.3 Inorganic Nutrients	50
4.4 Field Measurements	55
5.0 Discussion	59
5.1 Water Column Stratification	59
5.2 Light Depth Measurement	61
5.3 Primary Production and Respiration.....	62
5.4 BOD Discrepancy	64
5.5 Phytoplankton and Nutrient Cycling	66
6.0 Conclusions.....	68
7.0 References	70
Chapter 3: Conclusions and Future Directions	74
1.0 Conclusions.....	74
2.0 Future Directions.....	75

List of Figures

Chapter 1

1.1 Map of the Columbia River basin.....	2
1.2 Discharge in the main stem, Willamette, and other tributaries.....	2
1.3 Map of the lower Columbia River estuary and study area.....	3
1.4 Conceptual model of the open-water sensor method in the water column.....	9
1.5 Example of light attenuation with depth.....	22

Chapter 2

2.1 Sensitivity analysis of open-water respiration calculations to wind and current.....	41
2.2 Comparison of BOD and open water results of production and respiration.....	43
2.3 Regression analysis of sensor vs. BOD estimates of GPP.....	44
2.4 Five-day BOD bottle incubations compared with hourly estimates.....	45
2.5 Comparison of BOD ₅ and DOM concentrations.....	45
2.6 Temperature and turbidity.....	46
2.7 Regression analysis of sample vs. sensor chlorophyll <i>a</i> measurements.....	47
2.8 Chlorophyll <i>a</i> measurements.....	48
2.9 Regression analysis of chlorophyll <i>a</i> between depths.....	48
2.10 Particulate organic carbon flux.....	49
2.11 Inorganic nutrients.....	51
2.12 Regression analysis of sample vs. sensor nutrient measurements.....	52
2.13 Regression analysis of nutrients between depths.....	53
2.14 Dissolved inorganic nitrogen and net ecosystem metabolism.....	54
2.15 Depth of photic zone.....	55
2.16 Depth profiles.....	56
2.17 Percentage stratification between surface and depth.....	59

List of Tables

Chapter 2

2.1 Water column stratification measurements, Columbia River	57
2.2 Water column stratification measurements, Willamette River and other sites	58

Acknowledgements

I would like to extend my sincere thanks to my mentor Dr. Joseph Needoba for his guidance, support, patience, and inspiration, and for opening my eyes to the river as a dynamic, breathing system. Many thanks are also due to my committee members Drs. Tawnya Peterson and Byron Crump for their input, feedback, and expertise.

I am extremely grateful to all my colleagues in the Needoba Peterson lab for their moral support and camaraderie, including Bill Brady, Lyle Cook, Brittany Cummings, Taylor Dodrill, Dr. Rachel Golda, and Sally Landefeld – and especially Stuart Dyer and Dr. Sheree Watson for sharing their hands-on laboratory and field expertise and technical suggestions.

I am also incredibly thankful for the assistance with field work, calculations, and data entry provided by interns Camille Marshall and Kate Pippinger, and wish them the very best in their careers. Thanks are due as well to the hardworking current and former staff of OHSU Institute of Environmental Health, including Vanessa Green, James Mohan, and Dr. Michiko Nakano, without whom none of this would be possible.

Finally, I owe thanks to all my friends for their understanding and encouragement throughout this project – and to my parents, my brother, and all other family members for always being on my side.

“You can never step into the same river twice,

For other waters are ever flowing on to you.”

- Heraclitus

Abstract

Accurate estimation of phytoplankton primary production is an essential component of aquatic biogeochemistry because of its central importance in the cycling of inorganic nutrients, the production of 50% of the world's oxygen, the uptake of CO₂, and the production of particulate organic matter. This third product forms the basis of a substantial portion of the world's food webs, ecosystems, and fisheries. While primary production in marine, estuarine, and lentic systems has been extensively studied, the role that temperate rivers play in the world's biogeochemical cycles is not as well documented. As fast moving, dynamic environments, rivers present a unique set of challenges and often defy simplistic static attempts to quantify their trophic activity. Nevertheless, seasonal production and respiration follow patterns that can be understood as they relate to day length, temperature, river discharge, and water column stratification.

In the Columbia River basin, investigations are underway to uncover the seasonal dynamics of phytoplankton production and their importance in the ecosystem of the estuary. Evidence is mounting that hydroelectric dams on the Columbia impact plankton growth by increasing water residence times and temperatures, as well as settling and trapping of silt. These impacts lead to an increase in water column light availability and subsequently to large spring blooms that act to draw inorganic nutrients out of the water column and generate a large load of organic carbon, which is then transported downriver to feed bacterial production in the lower estuary. Monitoring of this process is made possible by an array of remote biogeochemical sensors as part of the Center for Coastal Margin Observation & Prediction (CMOP). These sensors allow continuous recording of oxygen, nutrient, and hydrological data necessary for calculating plankton production. However, because the sensors rest at a fixed depth, estimates of whole system production and respiration rely on an assumption that the entire water column is homogeneously mixed. This thesis is both an attempt to empirically test that assumption using field measurements – and having done so, to use the sensors to accurately track the metabolic dynamics of the lower Columbia and its tributary the Willamette River, in order to estimate the total daily export to the

estuary of particulate organic carbon throughout an entire year. The investigation revealed that both rivers are sufficiently well-mixed throughout the year to allow chemical changes anywhere in the water column to be detected by a sensor fixed at any depth. Calculations of net ecosystem metabolism showed that the Columbia is a net exporter of organic carbon for most of the year, with the exception of late summer and early fall, while the Willamette is comparatively inactive most of the year but experiences an abrupt shift in trophic state during late summer blooms. In summer 2017, this shift was evident in a marked increase in primary production, coupled with an even stronger respiration signal, resulting in net heterotrophy, followed by a sudden decline in biological activity in mid-August.

A central finding of this thesis is that hourly rates of pelagic aerobic respiration captured by BOD experiments consistently do not reflect whole-system respiration estimates based on sensor measurements, providing strong evidence that aerobic respiration in the Columbia and Willamette is largely accounted for by non-pelagic communities.

CHAPTER 1

Introduction

1.0 Overview of the Columbia River System

1.1 Hydrography

The Columbia River is the second largest river drainage in the continental United States, and the largest river discharge into the eastern North Pacific Ocean (Simenstad et al. 1990) (Figure 1.1). The major contribution to water runoff that defines the seasonal hydrograph is the spring freshet, an acute, regular event caused by winter snowmelt. In the lower Columbia River estuary, a five to tenfold increase in tributary input is observed during winter months due to rainfall at low elevations such as the Willamette valley and other regional catchments (Simenstad et al. 1990). In particular, the Willamette River contributes approximately 15% of total discharge during the summer, and up to 65% in the winter (Kammerer 1990, Benke & Cushing 2011, Wunsch et al. 2016). Thus, the seasonal hydrograph of the lower Columbia River is characterized by episodic high discharge events in winter, the spring freshet between April-July, and relatively low flows in summer and fall (Figure 1.2). The Columbia River Estuary (CRE) is defined as the tidally-influenced region downstream of Bonneville Dam (Figure 1.3) and is composed of freshwater and marine components. Compared with smaller coastal estuaries in the Pacific Northwest, the Columbia is much more river- as opposed to marine-dominated (Lara-Lara et al. 1990) and typically functions as a salt-wedge estuary. Owing to the large discharge of the Columbia, the water residence times are relatively short (Kärnä & Baptista 2016). The Columbia is a major point source for organic carbon export into the California Current upwelling system (Alin et al. 2012).



Figure 1.1: Map of the Columbia River basin, including watershed area and major tributaries. Source: Wikimedia Commons, <https://commons.wikimedia.org/wiki/File:Columbiarivermap.png>

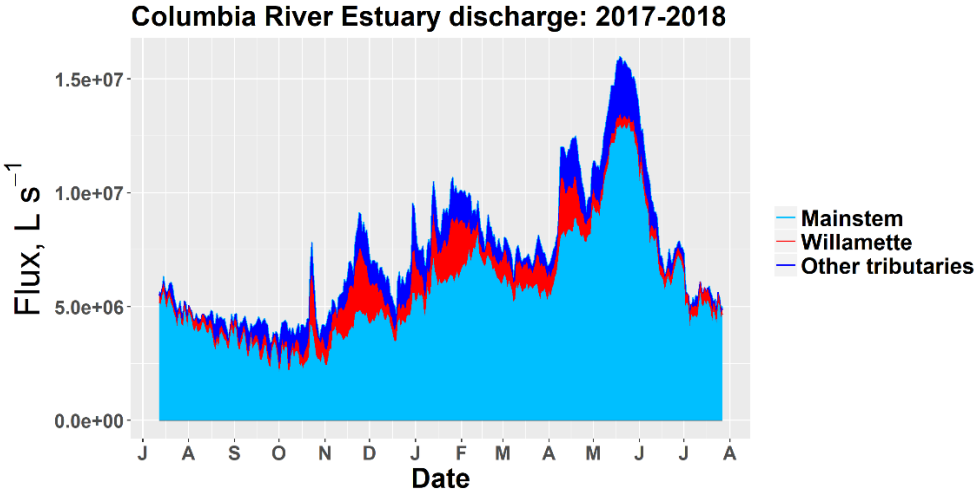


Figure 1.2: Relative discharge contributions through the Columbia river estuary, 2017-2018. Data for the mainstem and Willamette were downloaded from USGS sensors in downtown Portland OR and Vancouver WA, respectively. Total discharge data, including all major tributaries downstream of the confluence with the Willamette, are downloaded from the SATURN 05 sensor at the Beaver Army Terminal site near Cathlamet WA.

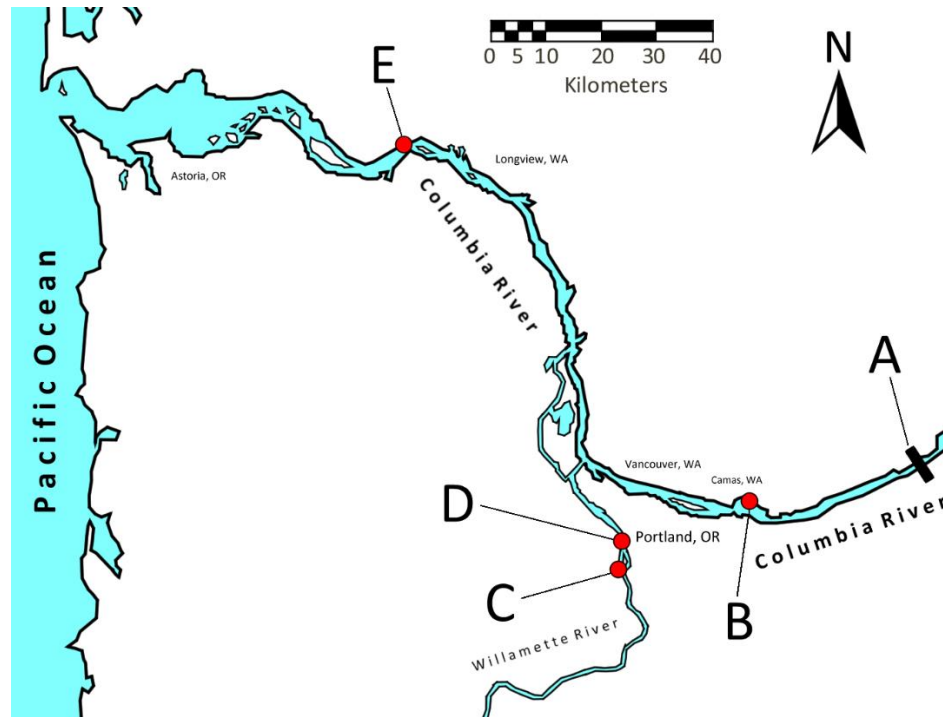


Figure 1.3: Map of the Columbia River estuary from the Bonneville Dam (A) to the river mouth. (B) CMOP SATURN-08 sensor and field sampling site for the lower Columbia River at Port of Camas-Washougal WA. (C) Field sampling site for the Willamette River at Willamette Park in Portland OR. (D) CMOP SATURN-06 sensor, at the Morrison Bridge in downtown Portland OR. (E) CMOP SATURN-05 sensor at Beaver Army Terminal (BAT) site.

1.2 Hydroelectric Dams and the Greening of the Columbia

A major anthropogenic influence on the Columbia River was the construction of dams during the twentieth century for the purposes of irrigation, flood control, transportation, and hydroelectric power generation. Currently there are 14 dams on the mainstem of the Columbia and more than 400 dams in the watershed (Weitkamp 1994). The economic benefits of dams in the Columbia drainage are far reaching and include the generation of 29 GW – or over 40% of all hydroelectricity in the United States (Lillis 2014), thousands of square kilometers of irrigated and flood-controlled land (Bloodworth & White 2008), and the opening of continuous navigable waterways from the Pacific Ocean to the interiors of Oregon, Washington, British Columbia, and Idaho (NPCC 2018).

Dams have had numerous, well-described impacts on the hydrology, ecology and biogeochemistry of rivers. These include changes to the hydrograph, migratory fish impacts, warming water temperatures, alterations in sediment loads, and changes in nutrient cycles, such as an increase in drawdown of reactive nitrogen and phosphorus during spring phytoplankton blooms, and the subsequent settlement and trapping of diatom-fixed amorphous silica (Triplett et al. 2012). In the Columbia River, the hydrograph changes are comprised of a 15% total reduction in flow and a 40% reduction of peak freshet flow since flow management first began in 1970 (Naik & Jay 2005). The storage of water in dam-controlled reservoirs and reduction of flood events leads to an increase in residence time above the dams, which allows warming of the water as well as silt settling and a subsequent reduction in sediment loads downstream of the dams (Simenstad et al. 1992, Weitkamp 1994). Migratory fish including salmonids (*Oncorhynchus spp.*) have been largely impacted by dams by the necessity of artificial fish passages and hatchery rearing, resulting in a simplification of their life histories and population age structures (Bottom et al. 2005). The CRE has also undergone significant changes, in particular to the habitat and biological productivity of the ecosystem. Human activities such as dredging, dike construction, and filling of marshland have caused an overall deterioration of intertidal habitat and the associated food webs upon which juvenile salmonids and many other species depend (Weitkamp 1994).

A less-well understood consequence of dams and habitat loss in the CRE is the role of pelagic primary production by phytoplankton. First documented in the 1960's, diatoms and other phytoplankton are distributed throughout the reservoirs and river reaches of the system. In un-dammed rivers (such as the Fraser River in British Columbia) the turbidity due to sediment greatly limits phytoplankton growth primarily due to light limitation (Vannote et al. 1980). However, for the Columbia it is postulated that the longer water residence times in dam-controlled impoundments lead to the settling and trapping of silt, which lowers turbidity in the water and increases available light for photosynthesis (Sullivan et al. 2001). The pattern of phytoplankton biomass in the Columbia follows the typical seasonality of temperate lakes, i.e. in spring and early summer, as daylength increases, phytoplankton blooms are observed, followed by

nutrient limitation and lower biomass in summer (Maier & Peterson 2014). This process has contributed to the observed 150% increase in total phytoplankton since the 1870s (Weitkamp 1994). The changes to the pelagic ecosystem leading to an increase in phytoplankton likely entail higher production of autochthonous organic carbon, which potentially enters the food web or is transported to the estuary and coastal ocean. The degree to which phytoplankton have altered the ecosystem of the CRE has not been adequately characterized, but may alter carbon and nutrient fluxes, and result in the export of particulate organic carbon through the estuary and the increased drawdown of inorganic nutrients. However, the pelagic food web supported by this increase in available organic carbon may be largely unavailable to juvenile salmon, which habitually rely on grazing- and macrodetritus-based food webs (Dahm et al. 1981, Weitkamp 1994, Sullivan et al. 2001, Bottom et al. 2005, Maier & Simenstad 2009).

2.0 Aquatic primary production

2.1 General Principles

Primary production by photosynthesis is the foremost process by which organic carbon is made available for consumers in the environment, and by which molecular oxygen is produced. In marine, lentic, and lotic ecosystems, the vast majority of primary production is achieved by photosynthetic phytoplankton (Falkowski & Raven 2007). The rate of primary production is thus a direct product of the growth of phytoplankton biomass, which is controlled by a number of abiotic factors – chiefly, the availability of labile inorganic nutrients, accessible sunlight, and optimal temperature. The process represents the direct input of photochemical energy and complex organic molecules into an ecosystem (Redfield 1958, Bender et al. 1987, Cloern et al. 2014). Organic matter production by phytoplankton throughout the world directly supports marine and aquatic food webs, as well as fisheries and other human industries that depend on them (Pauly & Christensen 1995), but excessive production events can also lead to an increase in detrital biomass and subsequent oxygen consumption during bacterial respiration, causing hypoxic “dead zones” in stratified waters that harm benthic fauna (Cloern 2014, Murrell et al. 2017).

Although dynamic on both a daily and annual scale, the metabolic regimes of rivers can be understood in terms of some general principles. Photosynthesis, the engine that feeds much of life on earth, is powered by photons interacting with the photosystems of a variety of organisms, many of them pelagic phytoplankton such as diatoms, dinoflagellates, and cyanobacteria. The electrochemical energy from the photons provides the redox potential to oxidize a molecule of water and reduce a molecule of CO₂, the end result of a series of reactions called the light reactions and the Calvin Cycle. The main products of this process are molecular oxygen (O₂) and the fixation of inorganic carbon atoms from CO₂ into an organic form, namely glucose (Falkowski & Raven 2007) (Equation 1.1).



Equation 1.1: General stoichiometry of photosynthesis. 6 molecules of CO₂ and H₂O result in the net production of 1 glucose molecule (C₆H₁₂O₆) and 6 O₂ molecules (Falkowski & Raven 2007).

Cellular aerobic respiration consists of a reverse stoichiometry, whereby oxygen and organic carbon are consumed and CO₂ is produced. These two processes, then, may be coupled both within a single cell and in aggregate across an entire ecosystem. Rates of photosynthesis are highest where light is most available, up to a level of radiation at which saturation of the photosystem and photoinhibition occur. In stratified waters, this means that the lack of vertical transport will ensure that most oxygen produced remains near the surface.

Aquatic primary production is a principal component of a larger ecosystem parameter, called Net Ecosystem Metabolism (NEM). This can most easily be understood as the balance between daily Gross Primary Production (GPP, measured in total biological oxygen production) and the Ecosystem Respiration (ER, measured in biological oxygen demand by all organisms). If GPP in a given system is greater than ER, NEM is a positive value, and more oxygen and organic carbon are being produced per

day than consumed. If ER is greater, then NEM is negative, and the system is acting as an oxygen and organic carbon sink rather than a source (Equation 1.2).

$$\mathbf{NEM = GPP - ER}$$

Equation 1.2: Conceptual formula for the balance of gross primary production and ecosystem respiration, as the term Net Ecosystem Metabolism (Caffrey 2003, Staehr et al. 2010).

Because photosynthesis is directly coupled to the fixation of autochthonous organic carbon from CO₂, a system in which GPP exceeds ER represents a source of organic carbon, and is termed *autotrophic*. Likewise, because growth and respiration by aerobic organisms entail the oxidation of organic carbon into CO₂, a system in which ER exceeds GPP is referred to as *heterotrophic*, and relies more on external, allochthonous organic carbon inputs. The balance of these terms, then, provides a convenient index of the *trophic state* of an aquatic ecosystem (Odum 1956, Caffrey 2003, Staehr et al. 2011, Needoba et al. 2012).

Estuaries and coastal ecosystems may have a positive NEM value, and thus be autotrophic, when runoff or upstream inputs provide high inorganic nutrient loads that fuel primary production; likewise, if a system receives runoff rich in detrital organic matter, a negative NEM, and thus heterotrophy, can result (Caffrey 2003, 2004). Therefore, while ER may increase or decrease in tandem with GPP due to the availability of phytoplankton-produced organic matter and labile organic nutrients (Crump et al. 2017), a significantly higher input of allochthonous dissolved organic matter can weaken or entirely decouple this relationship. Rivers in temperate latitudes that are relatively large, have sufficient light penetration, and in which disturbance occurs infrequently, tend to have regular annual productivity patterns that closely match the growing seasons of terrestrial ecosystems. Conversely, rivers that are frequently flooded or that experience other forms of disturbance have peaks that do not correlate with such patterns (Bernhardt et al.

2017). Rivers tend to follow an NEM gradient, from smaller shaded headwaters dominated by heterotrophy, to large fast-flowing lower reaches that are more autotrophic (Vannote 1980).

2.2 The Mixing Question

While primary production in marine, estuarine, and lentic environments has been extensively studied, the literature examining rivers is comparatively sparse. A central issue for determining factors involved in primary production in rivers concerns the physical mixing of the water column. In stratified systems, such as lakes and the open ocean, seasonal temperature patterns lead to changes in density stratification that control the depth of the upper mixed layer and thus the zone in which phytoplankton can grow. In such systems, phytoplankton tend to stay close to the surface to achieve adequate light for photosynthesis, but are known to migrate to depth for nutrient acquisition. A common assumption of rapidly flowing rivers is that sufficient turbulent mixing renders the water column entirely homogeneous. In this environment, particle concentrations and biogeochemical changes would be vertically dispersed throughout the water column on a relatively short timescale (e.g. less than 1 hour). The result would be that phytoplankton experience light conditions that fluctuate depending on their proximity to the surface, and likely experience light levels that are related to the depth of light penetration. Conceptually, a sensor recording water quality data near the surface of the ocean or a relatively deep, stratified lake would only be able to assess conditions near the surface, and couldn't be used to directly describe biogeochemical activity at lower depths (Figure 1.4). However, in turbulent river systems it is possible for representative conditions to be accurately measured by a sensor no matter what depth it is positioned at (Odum 1956, Needoba et al. 2012, Bernhardt et al. 2017).

In summary, a major control on phytoplankton growth in large rivers is likely the extent to which particles (including phytoplankton cells) are mixed throughout the water column, and the extent to which mixing creates a homogeneous environment that allows for the use of *in situ* sensors to adequately track biogeochemical and physical conditions at any depth. Water column homogeneity has not been empirically tested for the Columbia and Willamette rivers and is therefore a central research question of

this thesis, and is directly related to the accurate interpretation of remote sensor data and estimates of GPP and ER that are the subjects of this investigation.

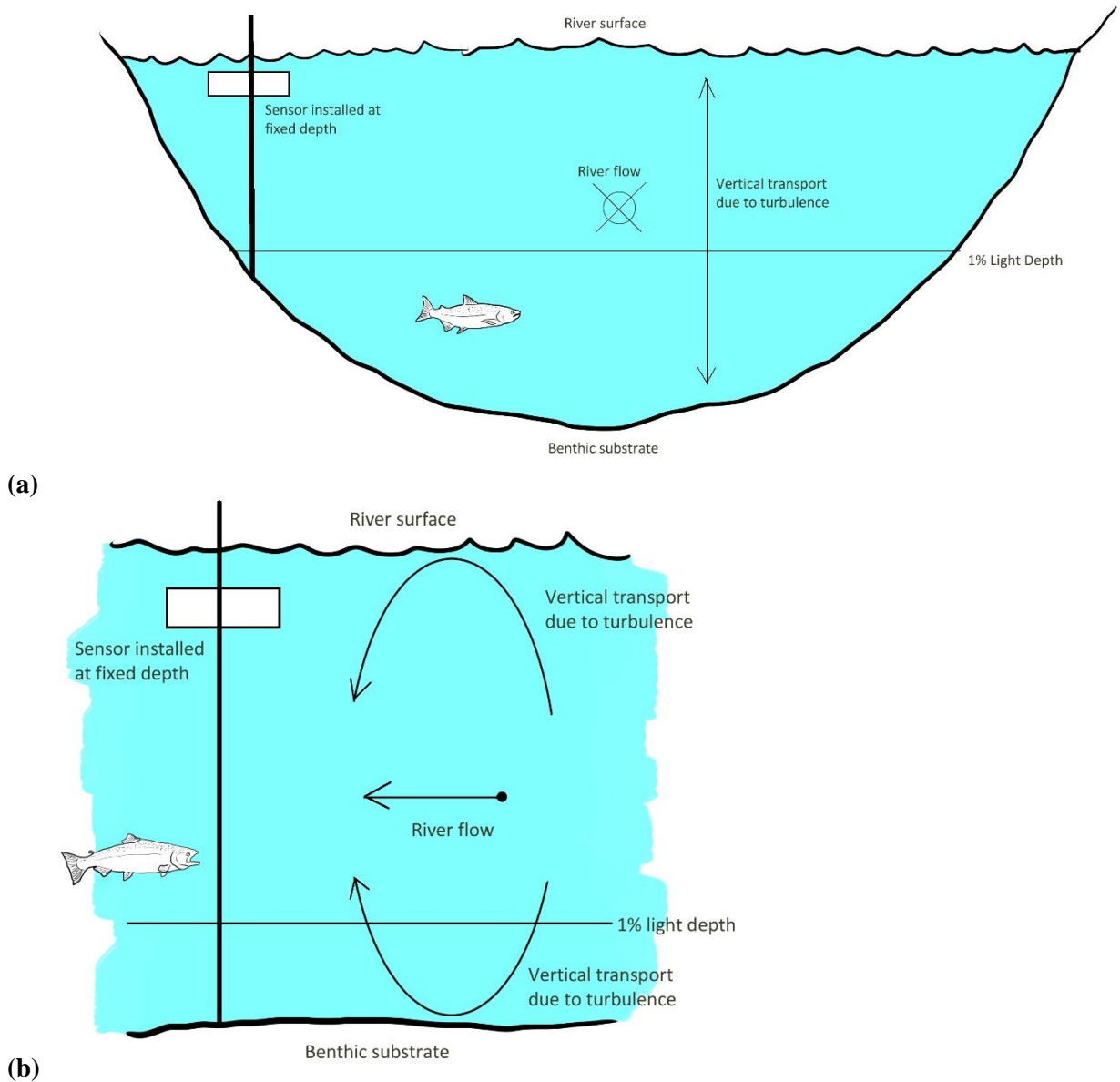


Figure 1.4: (a) Conceptual model of a cross section of a river, made perpendicular to flow direction. A biogeochemical sensor is installed at a fixed depth, recording water quality data at that depth. Even though phytoplankton production occurs above the 1% light depth, turbulence from the river flow rapidly transports the products of production and respiration throughout the water column, allowing detection by the sensor. (b) Cross section of the same river made parallel to the flow direction.

3.0 Measuring Aquatic Primary Production in Rivers

3.1 BOD “Light/Dark” Incubation Method

Conventionally, primary production can be measured by separating a water sample into aliquots designated “light” and “dark”, measuring their concentration of dissolved oxygen (DO), sealing and incubating the samples for a specific time interval at temperatures meant to closely approximate *in situ* conditions, and then measuring them again and calculating the rate of change. The “light” group should be incubated under full spectrum lighting to simulate solar radiation, and the “dark” group should be incubated with no light exposure. The change in DO under light conditions represents an estimate of *net primary production* (NPP) rates during daylight, and the change under dark conditions represents the average rate of ER assumed to take place over a diel cycle. It is here assumed that rates of production and respiration in a sealed sample will follow a non-linear pattern when incubated under steady light and temperature conditions (as nutrients become depleted in a “light” sample, or as dissolved oxygen and available organic carbon become depleted in a “dark” sample), so hourly estimates of *in vivo* rates should only be extrapolated from the first several hours of the incubation.

Because water temperature changes throughout the day and the year, it may not always be feasible to exactly match the environmental temperature in the incubation experiments. Since respiration rates vary considerably with water temperature, it is necessary to adjust measured hourly rates of respiration to reflect this. It is generally accepted that bacterial respiration tends to roughly double for each 10°C increase in temperature. However, actual rates vary widely with species assemblage, environment, and temperature range. The rate of metabolic change for a given sample is described by its Q_{10} value, the ratio of change between rates given a 10°C increase in temperature (Lampert 1984, Apple et al. 2006) (Equation 1.3a). With a known Q_{10} value and environmental temperature data, a Biochemical Oxygen Demand (BOD) measurement made in the laboratory can be adjusted to approximate its actual

rate under *in vivo* conditions (Equation 1.3b). While temperature may also affect the rate of production, respiration has been shown to respond more readily in some cases (Tait & Schiel 2013).

$$(a) \quad Q_{10} = (R_2 / R_1)^{(10^\circ\text{C} / T_1 - T_2)}$$

$$(b) \quad R_2 = R_1 * Q_{10}^{(T_2 - T_1 / 10^\circ\text{C})}$$

Equation 1.3: (a) Determination of Q_{10} coefficient, where R_1 and R_2 are the experimentally determined respiration rates at temperatures 1 and 2 (T_1 , T_2), respectively. (b) Use of the Q_{10} coefficient to predict a respiration rate (R_2) at a new temperature (T_2), given the measured respiration rate (R_1) at temperature T_1 (Lambert 1984).

An estimate of total biochemical oxygen demand over a period of five days is also frequently reported. This value, referred to as BOD₅, is made by first letting a sample's temperature stabilize at 20°C, measuring DO, leaving it in darkness at 20°C for five days (± 4 hours), and then measuring DO again (Delzer & McKenzie 2003). The sample may be incubated at a temperature other than 20°C to better reflect *in situ* conditions, but we stress here that results may not be comparable with BOD₅ measurements in other investigations.

Because *in situ* light levels vary throughout the day, the full spectrum lighting for incubation of surface samples should be set at an intensity and distance from the sample to approximate an average level of photosynthetically active radiation (PAR) experienced near the water's surface during daylight hours. To simulate conditions at other depths, neutral density screening can be used to lower the amount of PAR affecting the sample. Longer wavelengths of light are absorbed more rapidly in water than shorter ones (Falkowski & Raven 2007); however, at the relatively shallow depths typically considered in rivers, this difference is assumed to be negligible.

Several sources of error are inherent in BOD measurements. It is typically assumed that enclosure in a glass bottle does not alter phytoplankton behavior in ways that might significantly affect results (Staeher et al. 2010, Murrell et al. 2018); however, some effects are worth noting here. Respiration values in a “dark” bottle may not be representative of the rates in a “light” one due to the tendency of bacterial respiration to increase in tandem with phytoplankton growth, as well as an increase in respiration caused by the growth of the phytoplankton themselves. Depending on species assemblage, an increase in phytoplankton cell count may also increase the available surface area for bacterial growth due to the silica tests grown by diatoms, which often act as a substrate for bacteria to adhere to. However, the research demonstrating this (Pratt & Berkson 1959) dealt with 2-day BOD measurements of primary production, rather than the hourly timescales described here. It is also possible that respiration rates captured in bottle samples may be less than rates estimated from sensor data, because the BOD method captures only pelagic respiration, and there may be significant sources of respiration from benthically-adhered microbes that are unaccounted for in BOD-based calculations (Odum 1956, Van de Bogert et al. 2007).

3.2 Sensor-based open water method

Historically, high-resolution measurements of primary production in a given body of water were carried out in a 24-hour period of water sampling to find the diel change in oxygen and so quantify GPP and ER. However, this process is labor-intensive and difficult to carry out for longer periods than a single diel cycle, and does not provide a fully continuous time series. A preferable alternative that has become common in water quality science is the use of remote biogeochemical sensors. These robust *in situ* platforms provide not only dissolved oxygen data, but other measurements including current, nutrients, salinity, and chlorophyll. They require only occasional maintenance, and show promise in greatly increasing the logistical and technical capacity of the aquatic scientist (Needoba et al. 2012, Murrell et al. 2018).

Estimating primary production using *in situ* sensors, in its simplest sense, involves measuring the hourly change in dissolved oxygen and using this to infer the overall metabolic balance of the system.

Diurnal photosynthesis rates by phytoplankton typically follow well established patterns. The maximum rate of positive change in biogenic oxygen is immediately after sunrise and the maximum negative rate occurs after sunset. Photosynthesis usually exceeds respiration from mid-morning until noon, so oxygen concentration is observed at its maximum during the afternoon hours, and reaches a minimum before dawn (Odum 1956, Caffrey 2003, 2004). With the assumption that the rate of aerobic respiration recorded at night remains the same during the day, it is then possible to add the oxygen respired during the day to the NPP to obtain GPP – that is, the total amount of oxygen produced during daylight hours regardless of whether it was respired by organisms or transpired out of the system. It is always assumed that biological oxygen production during nighttime hours is zero (Odum 1956).

Given a continuous hourly timeseries of dissolved oxygen concentration and saturation, it is necessary to separate biological fluxes of oxygen from physical ones. This can be achieved using the protocol by Needoba et al. (2012). All calculations here are for hourly intervals. First, the rate of diffusion of oxygen between the water and the atmosphere is determined. This is dependent on both the *oxygen gradient* (the concentration of dissolved oxygen relative to equilibrium with the atmosphere, and thus its tendency to diffuse into or out of a given body of water) and the *piston velocity* (the flux caused by current and wind velocity). To find the extent to which oxygen diffusion is impacted by piston velocity, the influence of wind speed on piston velocity (k_{wind}) should be determined. This is found using the recorded wind speed and the Schmidt number – that is, the ratio of viscous diffusion rate to mass diffusion rate (Equation 1.4).

$$(c) \quad k_{wind} = 0.31 * u_{10}^2 * (Sc / 660)^{-0.5}$$

$$(d) \quad Sc_0 = 1800.6 - 120.1T + 3.7818T^2 - 0.047608T^3$$

Equation 1.4 (previous page): (a) Determination of wind-caused O₂ diffusion (k_{wind}) in cm h⁻¹, where u_{10} is wind speed at 10 meters above the water surface and Sc is the Schmidt number of O₂. **(b)** Formula to determine the Schmidt number of oxygen (Sc_O) in fresh water, where T is water temperature in °C.

In addition to k_{wind} , the magnitude of piston velocity is also determined by k_{flow} , the diffusion that results from turbulence caused by flowing water interacting with the benthic substrate. This value depends on water velocity rate, water column depth, and the molecular diffusion of oxygen. This latter term is a function of the association factor of water, the molar weight of water, water temperature, the molar volume of water at boiling point, and the dynamic viscosity of water, which is itself a function of temperature (Equation 1.5).

$$(a) \quad k_{flow} = (UD / h)^{0.5} * 3600$$

$$(b) \quad D = 7.4 * 10^{-8} * (xM)^{0.5} T / \eta V^{0.6}$$

$$(c) \quad \eta = (2.414 * 10^{-2}) * (10^{(247.8 / T - 140)})$$

Equation 1.5: (a) Formula to determine k_{flow} in cm h⁻¹, where U is the water speed in cm s⁻¹, D is the molecular diffusion of oxygen in cm² s⁻¹, and h is the total depth of the water column at the sensor. The equation is then multiplied by 3600 to convert the time interval from seconds to hours. **(b)** Molecular diffusion of oxygen (D), where x is the association factor of water (2.26), M is the molar weight of water (18 g mol⁻¹), T is water temperature in °K, η is the dynamic viscosity of water (reported in centipoise), and V is the molar volume of water at boiling point (25.6). **(c)** Dynamic viscosity of water (η), where T is water temperature in °K.

The terms k_{wind} and k_{flow} can then be combined to calculate piston velocity (vO₂) (Equation 1.6a), which – when combined the oxygen gradient – yield the concentration-dependent flux (FO₂), the total estimate of abiotic changes in oxygen concentration (Equation 1.6b). To calculate oxygen gradient, following

Henry's Law (Henry 1803), the partial pressure of oxygen and its solubility in water determine its equilibrium concentration with respect to the atmosphere. If a sensor logs the concentration of dissolved oxygen and its percentage saturation relative to an equilibrium of 100%, the equilibrium concentration of oxygen can be thus determined (Equation 1.6c).

$$(a) \quad vO_2 = k_{wind} + k_{flow}$$

$$(b) \quad FO_2 = -vO_2 * (O_{2meas} - O_{2sat})$$

$$(c) \quad O_{2sat} = [O_{2meas} / O_{2\%sat}] * 100$$

Equation 1.6: (a) Concentration dependent flux of oxygen (vO_2) in $m\ h^{-1}$, as the cumulative effects of k_{wind} and k_{flow} in $m\ h^{-1}$. (b) Concentration-dependent flux (FO_2) in $mmol\ O_2\ m^{-2}$, as a function of piston velocity (vO_2) and the difference between measured oxygen concentration (O_{2meas}) and oxygen concentration at saturation (O_{2sat}), in $mmol\ O_2\ m^{-3}$. (c) Calculation of the equilibrium concentration of dissolved oxygen (O_{2sat}) in $mmol\ L^{-1}$ relative to the atmosphere at sea level, where O_{2meas} is the recorded concentration of oxygen in $mmol\ L^{-1}$, and $O_{2\%sat}$ is the recorded percentage saturation relative to equilibrium with the atmosphere at sea level.

Having calculated FO_2 , it is then possible to discern the change in dissolved oxygen (DO) due to biological activity (BDO) for a given time interval, using measurements of DO and the depth of the water column (Equation 1.7). Assuming integration along a well-mixed water column, volumetric sensor measurements of DO given in $mmol\ m^{-3}$ can be made compatible with FO_2 estimates by multiplying by the water column depth at the sensor. These values can then be treated as areal measurements given in $mmol\ m^{-2}$, such that the whole water column is represented by a 1-meter square at the surface (Odum 1956, Needoba et al. 2012).

$$\mathbf{BDO}_t = (\mathbf{DO}_t - \mathbf{DO}_{t-1}) * h - \mathbf{FO}_2$$

Equation 1.7: Biological change in oxygen (*BDO*), where DO_t is the measured concentration of dissolved oxygen at a given time point, DO_{t-1} is the dissolved oxygen concentration at the previous time point, h is the depth of the water column in meters, and FO_2 is the concentration-dependent oxygen flux. DO concentrations are measured in mmol m^{-3} , while the BDO_t and FO_2 values are given in mmol m^{-2} . The time interval t is 1 hour.

Next, BDO can be used to determine the rate of aerobic respiration. Because the respiration rate cannot be directly separated from production by this method during the day, the hourly average of BDO during nighttime hours can be used, with the assumption that this respiration rate is constant throughout the diel cycle (Equation 1.8a). Respiration rates in some studies have been shown to be higher during the day – thus this technique might underestimate GPP and ER during daylight hours – but the common assumption is that this difference is negligible (Staehr et al. 2010, Needoba et al. 2012, Murrell et al. 2018). Also implicit in this technique is the assumption that all observed respiration rates are aerobic only and that photosynthesis occurs only at night (Needoba et al. 2012), so if the sensor reports a slightly positive value during nighttime periods, this can be assumed to result from a physical transport process and thus a value of zero should be substituted. Given an hourly estimate of ER, it is then possible to calculate the total amount of GPP during a diel cycle. This is accomplished by adding daytime NPP to the total estimate of respiration during daylight hours, thus accounting for all biologically produced oxygen regardless of its fate (Equation 1.8b).

$$\mathbf{(a)} \quad \mathbf{ER}_h = \Sigma(\mathbf{BDO}_n) / (n)$$

$$\mathbf{(b)} \quad \mathbf{GPP} = \mathbf{NPP} + (\mathbf{d} * |\mathbf{ER}_h|)$$

Equation 1.8 (previous page): (a) Estimation of average hourly respiration rate (ER_h), where n is the number of hours of darkness during a single diel period, and $\Sigma(BDO_n)$ is the sum of hourly respiration during nighttime hours. **(b)** Daily gross primary production (GPP), where NPP is the net biogenic change in oxygen during daylight hours, d is the number of daylight hours, and $|ER_h|$ is the absolute value of the estimated hourly respiration rate. All oxygen measurements are here given in $\text{mmol m}^{-2} \text{h}^{-1}$.

For whole system estimates, it may be convenient to keep the estimates as areal measurements (mmol m^{-2}); however, because the “light/dark” method described above (3.1) measures dissolved oxygen in volumetric units, it may also be necessary to convert the sensor-derived measurements to a per volume unit, by dividing the areal rate by the depth of the water column.

3.3 Chlorophyll

Chlorophyll *a* is an essential photopigment used by phytoplankton. It enables photosynthesis by absorbing photons in the blue and red portions of the electromagnetic spectrum (approximately 400-450 nm and 650-750 nm, respectively) and transferring the resultant energy by donating electrons to the *electron transport chain*, the process undertaken by a series of membrane-embedded protein complexes in the cell of a photosynthetic organism (Falkowski & Raven 2007). As the main pigment by which aquatic photosynthesis occurs, the concentration of chlorophyll *a* in an aquatic environment is commonly used as a proxy for phytoplankton biomass and photosynthetic activity.

In addition to being detectable by remote sensors, chlorophyll can be measured by field sampling. A non-acidified variation of the *in vitro* chlorophyll *a* determination protocol was used (Welschmeyer 1994). Samples should be taken in triplicate and kept in opaque bottles until returned to the laboratory, to prevent further photosynthesis by phytoplankton contained in the sample. Water samples are then run through 0.7 μm glass fiber filters placed on a vacuum filter manifold. The volume run through the filter can be as high as 250 mL, but water samples that are visibly turbid due to suspended silt or plankton should be filtered in volumes of 100 mL or less, to prevent clogging or oversaturation of the filter. Glass filters should be frozen between -20°C and -80°C until needed for extraction and analysis.

All procedures described below should be performed under minimum necessary ambient light. To begin extraction, frozen filters should be soaked in a 90% acetone solution, with each filter being placed in its own disposable glass culture tube. Volume of acetone used per tube should be a precise value. A single run of filters should include three blanks of 90% acetone. Once the filters have been immersed in acetone and their tubes capped, the tubes should be placed in a freezer in darkness for 2-24 hours for complete extraction. After that, filters are discarded, and an aliquot of the supernatant from each tube is poured into each sample cuvette. Measurements should be made in raw fluorescence units (RFU) using a fluorometer. To obtain the “uncorrected” chlorophyll *a* concentration value, several values are needed: the measured RFU of a sample, the average RFU of the three blanks, the volume of whole water sample filtered, and the volume of acetone used in extraction (Equation 1.9a). Concentration of chlorophyll can be fitted to a linear function based on RFU, but for samples in which the measured fluorescence exceeds 1500 RFU, a linear function should only be used if the supernatant is diluted again and the dilution factor is accounted for (Equation 1.9b).

$$(a) \quad C_s = ((F_s - F_b - L_2) / L_1) * (V_a / V_s)$$

$$(b) \quad C_d = [((F_d - F_b - L_2) / L_1) * (V_a / V_s)] * DF$$

Equation 1.9: (a) Function to calculate sample concentration of chlorophyll *a* (C_s), in $\mu\text{g L}^{-1}$, from measured fluorescence (F_s), in RFU, where F_b is the mean fluorescence of the blanks in RFU, L_1 and L_2 are linear calibration constants (4.7825 and 2.3747, respectively), V_a is the volume of 90% acetone used in extraction, and V_s is the volume of the original sample which was run through the 0.7 μm glass filter. (b) Modified chlorophyll calculation function for samples in which fluorescence exceeds 1500 RFU, where F_d is the measured fluorescence of the sample after dilution in RFU and DF is the dilution factor used.

With an accurate calculation of chlorophyll concentration, a timeseries of chlorophyll can be made and compared with measurements taken by remote sensors. With sampling at multiple depths, the extent to which chlorophyll is mixed or stratified between depths can be quantified.

3.4 Inorganic Nutrients

During photosynthesis, phytoplankton cells draw reactive nitrogen and phosphorus from the water, in the form of nitrate (NO_3^-) and phosphate (PO_4^{3-}). The rate at which these nutrients are consumed is determined by the stoichiometry of the cells themselves – and while it varies considerably between species assemblages and ecosystems, a commonly used average is the Redfield Ratio of 1:16:106:138 P:N:C:O₂ (Redfield 1958). This means that for every atom of phosphorus consumed, 16 nitrogen atoms and 106 carbon atoms are incorporated into the cell, and 138 O₂ molecules are produced. Following Liebig's *Law of the Minimum* (Liebig 1840), the maximum growth rate of phytoplankton is controlled by whichever element deviates negatively from that ratio the most, making it the limiting nutrient (Redfield 1958).

In the Columbia River, both nitrate and phosphate concentrations rise during autumn and peak in winter. Throughout the spring and early summer, they are depleted until they reach their annual minima in late summer, as they feed the increasing phytoplankton growth during the spring bloom (Dahm et al. 1981). Nitrate rises to an average of around 25 μM in winter, and falls to around 5 μM in late summer. Phosphate reaches its maximum of 1 μM in winter, and drops to almost immeasurably small concentrations in late summer (Prahl et al. 1997, Sullivan 2001). The Willamette bears consistently higher concentrations of both nutrients throughout the year, with nitrate levels measured at up to 40 μM and phosphate in the 2-3 μM range (Prahl et al. 1997). Sullivan et al. (2001) suggested that because total phosphate depletion never occurs in the Columbia mainstem, the river is not nutrient limited; however, a secondary annual plankton bloom in June in the Columbia downstream of its confluence with the Willamette has been observed, possibly due to the injection of phosphate-rich water from the Willamette into the Columbia (Wünsch et al. 2016).

3.5 Photosynthetically Active Radiation

The autotrophic production of organic matter is limited to the upper region of the water column, termed the *photic zone*, in which sufficient *photosynthetically active radiation* (PAR) is available during the day to promote phytoplankton growth. Under conditions where nutrients required for primary production are not limiting, light availability can conceivably control primary production, with a deeper photic zone correlating with a greater GPP. Thus, in addition to nutrient availability, PAR can be a limiting factor on phytoplankton growth and activity (Redfield 1958, Vannote 1980). Conventionally, the photic zone is estimated to extend to the depth at which PAR has attenuated to one percent of surface incident light (Ryther & Menzel 1958, Falkowski & Raven 2007). When light passes through a liquid medium, there is a predictable attenuation with depth. In homogeneously-mixed waters, this follows a simple exponential decay function, the rate of which is exacerbated – as per the Beer-Lambert Law (Bouguer 1729, Lambert 1760, Beer 1852) – by the amount and type of suspended particulate matter (Lorenzen 1972, Bernhardt et al. 2017) (Equation 1.10).

$$(a) \quad I_z = I_0 * e^{-kz}$$

$$(b) \quad z = -\ln(1 / 100) / k$$

Equation 1.10: (a) Formula for the attenuation of light in a homogenous water column, where I_z is the illumination at a given depth z , I_0 is the surface illumination, and k is the decay coefficient of light in the medium (Lorenzen 1972). (b) Light attenuation formula, rearranged to predict the depth z at which PAR decays to 1% of surface illumination, given a light decay coefficient of k .

To determine the depth of the photic zone, a *light integration sphere* – an apparatus that quantifies the average PAR, measured in $\mu\text{mol photons m}^{-2} \text{s}^{-1}$ – can be employed. It should be linked to a terrestrial sensor that records surface incident light simultaneously. If the instrument does not also contain a CTD (conductivity, temperature, depth) sensor, it should be attached to one and lowered simultaneously, with

sufficient weight to prevent excessive horizontal drift in the river current. The assembly can be lowered for multiple casts, and if the CTD and light sphere are separate instruments, the descent should be stopped for at least 30 seconds at several pre-determined depths. By creating a recognizable “stepwise” pattern, data from the two instruments can more easily be combined. Upon touching the river bottom, the sensor should be allowed to rest for at least thirty seconds, and then raised, stopping several times on the ascent to further enable easy combination of data. Measurements should be carried out within two hours of noon, because low light angles earlier or later in the day can produce inconsistent data (Murrell et al. 2018).

The data for depth and light are then combined, and the timestamps for the two instruments are matched when cleaning the data. Data from the descending portion of the cast should be used, to ensure measurements do not reflect already disturbed portions of the water column, although a swift river current that rapidly mixes the water column may make this precaution unnecessary. These data are then divided into bins based on depth, with each depth bin corresponding to a range above and below a nominal depth, and each bin is then averaged. To account for variations in surface light such as clouds passing over the sun during the measurement, the resulting averages for the depth bins can then be normalized to the average surface light during a given cast (Equation 1.11).

$$I_{adj} = I_z * (A_z / A_{avg})$$

Equation 1.11: Formula for the normalization of PAR measurements to average surface light, where I_{adj} is the adjusted PAR value for a given depth, I_z is the initial PAR value for a given depth bin, A_z is the surface light measured during the cast where I_z values were measured, and A_{avg} is the overall average surface light during all casts on the sampling day.

The surface light-normalized values for each depth bin can then be averaged among all casts to produce a modeled light attenuation curve for that sampling day (Figure 1.5). Using Equation 1.10a, a value for the

light decay coefficient, k , can be derived. Using k , the depth of the photic zone can be determined by solving Equation 1.10b.

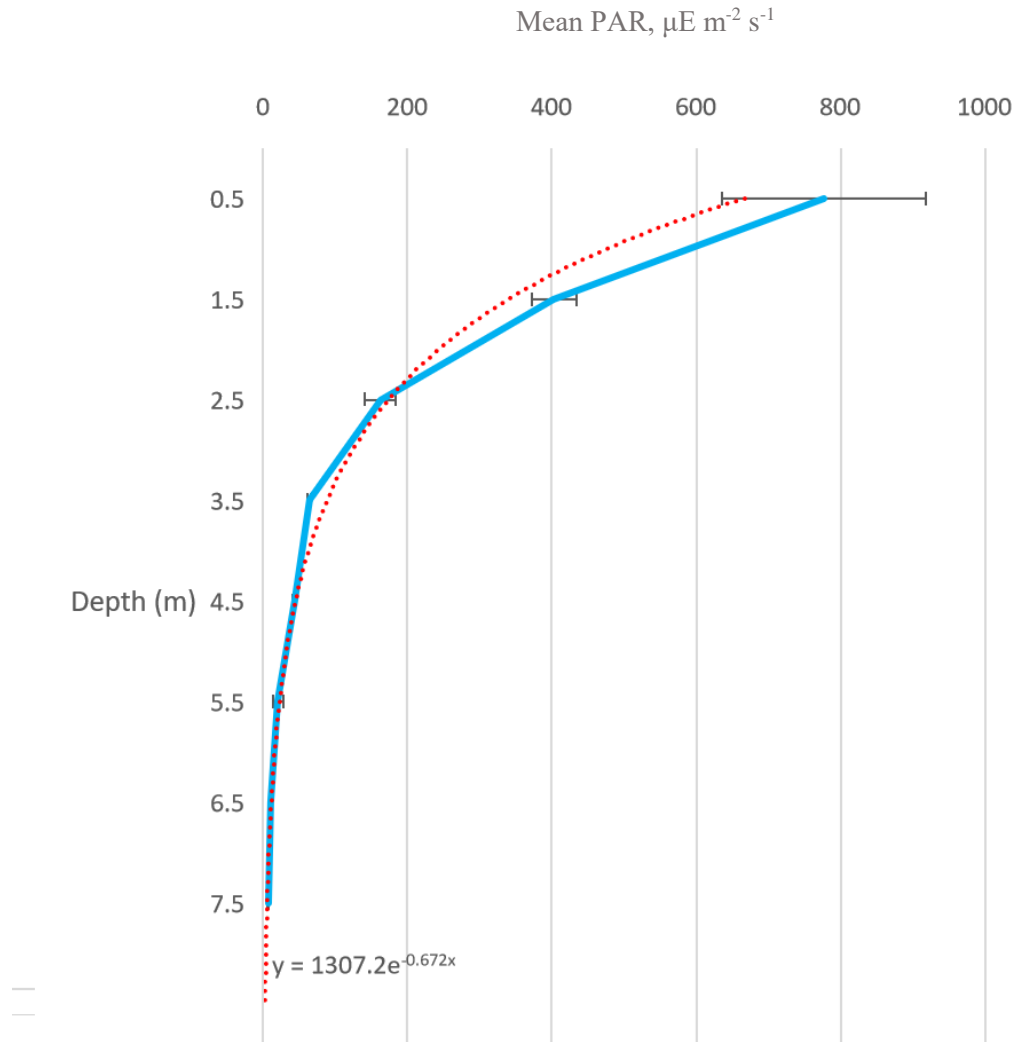


Figure 1.5: Example of a modeled light curve, the average of three separate casts taken at Port of Camas-Washougal, WA. Error bars are centered on the midpoint of each depth bin, and show that error is greater at shallower depths due to waves.

4.0 Study Rationale and Objectives

While a clear picture of net ecosystem metabolism in the Columbia and Willamette rivers is gradually taking form, many questions remain to be explored. Obtaining an accurate model of the trophic patterns in the rivers is crucial in the face of the changes in snowmelt, rainfall, and weather patterns that are predicted to occur within the next century (Hamlet & Lettenmaier 2000). While the impacts of these changes on the environment and economy of the Columbia system are far from certain, developing a better understanding of the spatial and temporal distribution of production and respiration will ensure the accuracy of current and future biogeochemical models. This study was undertaken to test the assumption that the water columns in both rivers are homogeneously mixed, to compare the accuracy of primary production estimates between those derived from *in situ* sensors and those derived from sample-based experiments, and to assess the seasonal patterns of the trophic states of the rivers. The mixing assumption is common both in interpretation of sensor data that come from a single depth, and sampling protocols that rely on whole water surface grabs. If the water column of either river is stratified, it would mean that present calculations of primary production there are inaccurate, and an accurate estimate would require the installation of sensors at multiple depths. Although some gaps exist in the data during the fall, this study was able to answer the question, showing that significant water column mixing does occur in both rivers. This is an important validation of many studies and models of the Columbia River system. In addition, the study encountered an unexpected but consistent discrepancy in the Columbia between total respiration as determined from sensors, and exclusively pelagic respiration as measured in BOD bottles, suggesting that the majority of aerobic respiration in the river may not be pelagic, but benthic in origin. Further research is needed to determine the cause of this result. The overall seasonal patterns observed largely matched predicted patterns, with increases in production and respiration, chlorophyll, and nutrient drawdown all corresponding with the spring blooms in both rivers, and the Columbia acting as a net source of organic carbon through much of the year. The Willamette varied, with low activity much of the year and a large bloom and corresponding heterotrophic event recorded in late summer.

5.0 References

Alin, S., Siedlecki, S., Hales, B., Mathis, J., Evans, W., Stukel, M., Gaxiola-Castro, G., Hernandez-Ayon, J.M., Juranek, L., Goñi, M., Turi, G., Needoba, J., Mayorga, E., Lachkar, Z., Gruber, N., Hartmann, J., Moosdorf, N., Feely, R., & Chavez, F. (2012). Coastal carbon synthesis for the continental shelf of the North American Pacific Coast (NAPC): Preliminary results. *Ocean Carbon and Biogeochemistry News*, **5**(1), 1-5.

Apple, J.K., Del Giorgio, P.A., & Kemp, W.M. (2006). Temperature regulation of bacterial production, respiration, and growth efficiency in a temperate salt-marsh estuary. *Aquatic Microbial Ecology*, **43**, 243-254.

Beer, A. (1852). Bestimmung der Absorption des rothen Lichts in farbigen Flüssigkeiten. (Determination of the absorption of red light in colored liquids). *Annalen der Physik und Chemie*, **86**, 78–88.

Bender, M., Grande, K., & Johnson, K. (1987). A comparison of four methods for determining planktonic community production. *Limnology and Oceanography*, **32**(5), 1085-1098.

Benke, A.C., & Cushing, C.E. (Eds.). (2011). *Rivers of North America*. Burlington, MA: Elsevier Academic Press.

Bernhardt, E., Heffernan, J., Grimm, N., Stanley, E., Harvey, J., Arroita, M., Appling, A.P., Cohen, M.J., McDowell, W.H., Hall, R.O., Jr., Read, J.S., Roberts, B.J., & Stets, E.G., Yackulic, C. (2017). The metabolic regimes of flowing waters. *Limnology and Oceanography*, **63**, 99-118.

Bloodworth, G., & White, J. (2008). The Columbia Basin Project: seventy-five years later. *Yearbook of the Association of Pacific Coast Geographers*, **70**, 96–111.

Bottom, D.L., Simenstad, C.A., Burke, J., Baptista, A.M., Jay, D.A., Jones, K.K., Casillas, E., & Schiewe, M.H. (2005). Salmon at river's end: the role of the estuary in the decline and recovery of Columbia River salmon. *NOAA Technical Memorandum NMFS-NWFSC-68*.

Bouguer, P. (1729). Essai d'optique sur la gradation de la lumière (Optical test on the gradation of light). Paris.

Caffrey, J.M. (2003). Production, respiration and net ecosystem metabolism in U.S. estuaries. *Coastal Monitoring through Partnerships: Proceedings of the Fifth Symposium on the Environmental Monitoring and Assessment Program (EMAP)* Pensacola Beach, FL, U.S.A., April 24-27, 2001, 207-219.

Caffrey, J.M. (2004). Factors controlling net ecosystem metabolism in U.S. estuaries. *Estuaries*, **27**(1), 90-101.

Cloern, J., Foster, S., & Kleckner, A. (2014). Phytoplankton primary production in the world's estuarine-coastal ecosystems. *Biogeosciences*, **11**(9), 2477-2501.

Crump, B., Fine, L., Fortunato, C., Herfort, L., Needoba, J., Murdock, S., & Prah, F. (2017). Quantity and quality of particulate organic matter controls bacterial production in the Columbia River estuary. *Limnology and Oceanography*, **62**(6).

Dahm, C.N., Gregory, S.V., & Park, P.K. (1981). Organic carbon transport in the Columbia River. *Estuarine, Coastal and Shelf Science*, **13**(6), 645-658.

Delzer, G.C., & McKenzie, S.W. (2003). Five-day biochemical oxygen demand. *United States Geological Survey Techniques of Water-Resources Investigations Report, Book 9-A7*(3), 1-21.

Falkowski, P.G., & Raven, J.A. (2007). *Aquatic Photosynthesis*. Princeton: Princeton University Press.

Graham, Daniel W. (2015) Heraclitus. In Zalta, E.N. (Ed.) *The Stanford Encyclopedia of Philosophy (Fall 2015 Edition)*, Retrieved from <https://plato.stanford.edu/archives/fall2015/entries/heraclitus>

Hamlet, A.F., & Lettenmaier, D.P. (2000). Effects of climate change on hydrology and water resources in the Columbia River basin. *Journal of the American Water Resources Association*, **35**(6), 1597-1623.

Henry, W. (1803). Experiments on the quantity of gases absorbed by water, at different temperatures, and under different pressures. *Philosophical Transactions of the Royal Society*, **93**, 29-274.

Kammerer, J.C. (1990). Largest rivers in the United States. *United States Geological Survey Water Fact Sheet, Open-File Report 87-242*.

Kärnä, T., & Baptista, A.M. (2016). Evaluation of a long-term hindcast simulation for the Columbia River estuary. *Ocean Modeling*, **99**, 1-14.

Lambert, J.H. (1760). *Photometria, sive de mensura et gradibus luminis, colorum et umbrae* (Photometry, or on the measure and gradations of light, colors, and shade). Augsburg.

Lampert, W. (1984). The measurement of respiration. *A Manual on Methods for the Assessment of Secondary Productivity in Fresh Waters, 2nd edn.*, 413-468. In Downing, J.A., & Rigler, F.H. IBP Handbook 17, Blackwell Scientific Publications: Oxford.

Lara-Lara, J., Frey, B., & Small, L. (1990). Primary production in the Columbia River Estuary: spatial and temporal variability of properties. *Pacific Science*, **44**(1), 17-37.

Liebig, J. von (1840). Organic chemistry in its applications to agriculture and physiology. In Playfair, L. (Ed.). London, UK.

Lillis, K. (2014). *The Columbia River Basin provides more than 40% of total U.S. hydroelectric generation*. Retrieved from United States Energy Information Administration, <https://www.eia.gov/todayinenergy/detail.php?id=16891>

Lorenzen, C. (1972). Extinction of light in the ocean by phytoplankton. *ICES Journal of Marine Science*, **34**(2), 262-267.

Maier, M.A., & Peterson, T.D. (2014). Observations of a diatom chytrid parasite in the lower Columbia River. *Northwest Science*, **88**(3), 234-245.

Maier, G., & Simenstad, C. (2009). The role of marsh-derived macrodetritus to the food webs of juvenile chinook salmon in a large altered estuary. *Estuaries and Coasts*, **32**(5), 984-998.

Murrell, M., Caffrey, J., Marcovich, D., Beck, M., Jarvis, B., & Hagy, J. (2018). Seasonal oxygen dynamics in a warm temperate estuary: effects of hydrologic variability on measurements of primary production, respiration, and net metabolism. *Estuaries and Coasts*, **41**(3), 690-707.

Naik, P.K., & Jay, D.A. (2005). Estimation of Columbia River virgin flow: 1879 to 1928. *Hydrological Processes*, **19**(9), 1807-1824.

Needoba, J., Peterson, T., & Johnson, K. (2012). Method for the quantification of aquatic primary production and net ecosystem metabolism using in situ dissolved oxygen sensors. In Needoba, J., Peterson, T., Johnson, K., & Tiquia-Arashiro, S. (Eds.), *Molecular Biological Technologies for Ocean Sensing*. Totowa, NJ: Humana Press.

Northwest Power and Conservation Council (2018). *Navigation*. Retrieved from <https://www.nwcouncil.org/reports/columbia-river-history/navigation>

Odum, H.R. (1956). Primary production in flowing waters. *Limnology and Oceanography*, **1**(2), 102-117.

Pauly, D., & Christensen, V. (1995). Primary production required to sustain global fisheries. *Nature*, **374**, 255-257.

Prahl, F., Small, L., & Eversmeyer, B. (1997). Biogeochemical characterization of suspended particulate matter in the Columbia River estuary. *Marine Ecology Progress Series*, **160**, 173-184.

Pratt, D.M., & Berkson, H. (1959). Two sources of error in the oxygen light and dark bottle method. *Limnology and Oceanography*, **4**(3), 328-334.

Redfield, A.C. (1958). The biological control of chemical factors in the environment. *American Scientist*, **46**(3), 205-221.

Ryther, J.H., & Menzel, D.W. (1958). Light adaptation by marine phytoplankton. *Limnology and Oceanography*, **4**(4), 492-497.

Simenstad, C.A., Jay, D.A., & Sherwood, C.R. (1992). Impacts of watershed management on land-margin ecosystems: The Columbia River estuary. In Naiman, R.J. (Ed.). *Watershed management: Balancing sustainability and environmental change*, 266–306. Springer-Verlag: New York, NY.

Simenstad, C.A., Small, L., McIntire, D.C., Jay, D., & Sherwood, C. (1990). Columbia river estuary studies: An introduction to the estuary, a brief history, and prior studies. *Progress in Oceanography*, **25**(1-4), 1-13.

Staehr, P., Bade, D., Koch, G., Williamson, C., Hanson, P., Cole, J., & Kratz, T. (2010). Lake metabolism and the diel oxygen technique: state of the science. *Limnology and Oceanography: Methods*, **8**, 628-644.

Sullivan, B.E., Prahl, F.G., Small, L.F., & Covert, P.A. (2001). Seasonality of phytoplankton production in the Columbia River: A natural or anthropogenic pattern? *Geochimica et Cosmochimica Acta*, **65**(7), 1125-1139.

Tait, L.W., & Schiel, D.R. (2013). Impacts of temperature on primary productivity and respiration in naturally structured macroalgal assemblages. *PLoS ONE*, **8**(9), 1-10.

Triplett, L.D., Engstrom, D.R., & Conley, D.J. (2012). Changes in amorphous silica sequestration with eutrophication of riverine impoundments. *Biogeochemistry*, **108**, 413-427.

Van de Bogert, M.C., Carpenter, S.R., Cole, J.J., & Pace, M.L. (2007). Assessing pelagic and benthic metabolism using free water measurements. *Limnology and Oceanography: Methods*, **5**, 145-155.

Vannote, R.L., Minshall, G.W., Cummins, K.W., Sedell, J.R., & Cushing, C.E. (1980). The river continuum concept. *Canadian Journal of Fisheries and Aquatic Sciences*, **37**(1), 130-137.

Weitkamp, L.A. (1994). A review of the effects of dams on the Columbia River estuarine environment, with special reference to salmonids. *Report to Bonneville Power Administration, Contract 227 DE_A179-93BP99021*.

Welschmeyer, N.A. (1994). Fluorometric analysis of chlorophyll *a* in the presence of chlorophyll *b* and pheopigments. *Limnology and Oceanography*, **39**(8), 1985-1992.

Wünsch, U., Koch, B., Witt, M., & Needoba, J. (2016). Seasonal variability of dissolved organic matter in the Columbia River: In situ sensors elucidate biogeochemical and molecular analyses. *Biogeosciences: Discussions*.

CHAPTER 2

Primary Production and Vertical Mixing in the Lower Columbia and Willamette Rivers

1.0 Abstract

The Columbia River is the subject of ongoing investigations to determine its role in carbon and nutrient export to the coastal ocean and the importance of autochthonous pelagic carbon production to the food web of the river. Evidence exists that the construction of dams during the 20th century is responsible for decreasing sediment loads that resulted in an increase in light penetration in the water column and phytoplankton-based primary production. This may be an important new source of organic carbon to the food webs of the lower estuary and coastal plume. However, the seasonal dynamics of phytoplankton-based primary production in the river have yet to be adequately characterized. In this investigation, our goal was to accurately determine the net production of organic carbon in the lower Columbia and compare it to the Willamette River as an example of an un-dammed river. Remote sensors used to make *in situ* estimates of production and respiration rates were employed, and weekly sampling was used to validate the sensor measurements. Since the sensors are placed at a fixed depth, whole-system estimates rely on the assumption that the water column is sufficiently mixed to prevent stratification. To test this assumption, we used a combination of vertical CTD depth profiles, BOD bottle experiments, and whole water samples of inorganic nutrients and chlorophyll *a* taken at two different depths at weekly intervals. We also measured photosynthetically active radiation and water column light attenuation in both rivers. Our results showed that the water columns in both rivers are uniformly mixed over short time scales and that light depths in the Columbia are relatively deep compared to other rivers. Our calculations of primary production demonstrate that the Columbia is consistently a net source of organic carbon, and the Willamette is a net sink. In addition, our estimates of respiration based on open-water sensor measurements and BOD incubations differed substantially, suggesting that respiration in the rivers is largely not pelagic.

2.0 Introduction

Understanding and quantifying the dynamics of aquatic primary production, the process by which photosynthetic phytoplankton generate organic carbon and produce roughly half of the world's atmospheric molecular oxygen (Nelson, accessed 8/20/18), is a fundamental aspect of ecosystem science and is crucial for many applications including: modeling the global carbon cycle (Field et al. 1998, Falkowski et al. 2000, Cole et al. 2007, Alin et al. 2012), predicting hypoxia events (Donner & Scavia 2007, Howarth et al. 2011), and tracking the availability of food for aquatic and marine ecosystems (Weitkamp 1994, Pauly & Christensen 1995, Bottom et al. 2005). Although primary production has been extensively studied in lakes, estuaries, and oceans, fewer investigations have been conducted on primary production in rivers.

The Columbia River is a system in which much remains to be learned about annual patterns of primary production and ecological responses to environmental change. Ongoing investigations have revealed the impact that silt trapping by hydroelectric dams has on increasing light availability and thus photosynthetic activity, causing the annual metabolism of the river to behave more like that of a temperate lake (Weitkamp 1994, Sullivan et al. 2001, Maier & Simenstad 2009, Gilbert et al. 2013, Maier & Peterson 2014). The result is an increase in phytoplankton-derived particulate organic carbon (POC) passing into the estuary, which can become suspended in the estuarine turbidity maximum (ETM) at the river's mouth and fuel bacterial secondary production (Crump et al. 2017). Given the typical high turbidity of the lower estuary, this source of POC is likely to be critical to supporting the estuarine food web. The degree to which this source of organic carbon reaches fish, including juvenile salmonids, is unclear, but may compete with the alternate source of primary production fueled by macro-detritus from the region's wetlands (Weitkamp 1994, Bottom et al. 2005). Although not conclusive, there is evidence that riverine primary production exceeds organic carbon respiration, thus the Columbia can be categorized as an autotrophic "green" river. Conversely, its major tributary the Willamette is not restricted by artificial impoundments, and is thought to experience lower levels of primary production due to higher silt

loads and light limitation, making it a heterotrophic “brown” river. The inorganic nutrients that fuel phytoplankton blooms in the Columbia instead pass through the Willamette largely unchanged, causing the Willamette to have significantly higher inorganic nutrient concentrations and loads (Sullivan et al. 2001).

Remote sensors are being used to track biogeochemical dynamics in the Columbia and the Willamette rivers (Kärnä & Baptista 2016). These sensors represent a positive development in aquatic science, as they enable constant high-resolution time-series measurements and need only occasional maintenance. Due to costs and logistics, sensors in the Columbia and Willamette rivers are deployed at only one depth in the water column, thus the measurements are only representative of the river if the entire water column is well mixed (Needoba et al. 2012). An important application of in situ sensors is for the measurement of Net Ecosystem Metabolism (NEM, Chapter 1). On a regional and global scale, the ability to calculate the trophic state of rivers is crucial, both for estimation of a system’s susceptibility to eutrophication and in tracking its impact on the global carbon cycle. Estimating the total carbon budget of a river based on changes near the surface recorded by the open-water method is reasonable if the water column is well-mixed, but will be inaccurate if spatial distribution of the water column is anything other than uniform. For example, in a highly stratified water column in which oxygen produced by photosynthesis is not well-mixed and remains concentrated in the photic zone, generalizing the results of fixed-depth open-water DO measurements to the whole water column would over-estimate the total rate of primary production in the system. Using this invalid assumption would lead to models of the total system that inaccurately report substantially higher rates of POC production, limiting their utility in carbon budget estimates.

We used in situ biogeochemical sensors, combined with weekly site visits to collect water samples, to validate and track seasonal changes in gross primary production (GPP) and ecosystem respiration (ER) in the two rivers. Our comparative approach allowed us to evaluate sensor-based estimates of production and respiration with sample-based ones over different seasons and river discharge

levels. This investigation allowed us to empirically test the water column mixing hypothesis, by comparing these values to sample-based estimates from two different optical depths in both rivers. We measured chlorophyll and inorganic nutrients at both depths to corroborate these results. We made sonde casts to determine the vertical profile of dissolved oxygen, salinity, and temperature to further test the mixing hypothesis. Additionally, we measured the depth of the photic zone, to determine if light limitation is an important controller of river primary production.

3.0 Materials and Methods

3.1 Sensor-based calculations

3.1.1 CMOP campaign and site description

We utilized two sensors in the Center for Coastal Margin Observation and Prediction (CMOP)'s Science & Technology University Research Network (SATURN), an array that spans the lower Columbia system. These sensors are CMOP's SATURN 08 in the Columbia River, and the United States Geological Survey (USGS)'s SATURN 06 in the Willamette River (USGS 14211720). SATURN 08 is suspended beneath a floating dock at the Port of Camas-Washougal marina in Washington State. This station is located at river mile 122 of the Columbia, upstream of the river's confluence with the Willamette and downstream of the Bonneville Dam. The site is suitable for this investigation because the sensor is exposed directly to the flow of the main stem of the Columbia. SATURN 06 is located at river mile 12.8 of the Willamette, and is attached to the Morrison bridge in downtown Portland. Both sensors' direct exposure to the main channel flow ensures that variations in water chemistry are likely to be representative of the river as a whole, and thus not locally influenced. We assume river biogeochemical cycles are homogeneous over large stretches of the river and as many physical variables are controlled as possible (Caffrey 2003). An example of a scenario in which physical variables are not controlled might involve one sensor being placed in a stratified eddy or slough and the other being placed in the main channel. It should be noted that SATURN 08 was undergoing maintenance and was not deployed between the months of October 2017 and February 2018.

3.1.2 Open water NEM Protocol

Gross primary production (GPP), Ecosystem Respiration (ER), and Net Ecosystem Metabolism (NEM) were determined following the protocols outlined in Chapter 1. Briefly, we measured the total amount of biologically-derived oxygen (BDO) produced during a day from the hourly change of dissolved oxygen (DO) using in situ sensors or bottle incubations. DO consumption via aerobic respiration is assumed to be nearly constant throughout day and night hours, therefore ER was determined via DO changes during night, and the rate was applied to the entire 24-hour period used for the calculations. Daytime increases in DO from photosynthesis represent a net change, thus by adding the absolute value of the estimated total respiration during daylight hours to the net primary production (NPP), the GPP can be calculated. Together, the balance of GPP and ER over 24 hours are a measure of NEM, or the *trophic state* of a given ecosystem during that day: if GPP is higher, the system is a net source of O₂ and autochthonous organic matter, and if ER is higher, the system is a net sink of O₂ and relies on allochthonous organic matter (Caffrey 2003, Staehr et al. 2010, Needoba et al. 2012,).

Sensor data were downloaded for SATURN 08 from the LOBO website [<http://columbia.loboviz.com>], and SATURN 06 data from the USGS website [https://waterdata.usgs.gov/nwis/inventory/?site_no=14211720]. Using the protocol by Needoba et al. (2012), we removed abiotic oxygen flux, which is the product of atmosphere-surface water gas diffusion, and is a function of water temperature, wind speed, and current velocity. Wind speed for SATURN 08 were downloaded from the nearby weather station at the Portland Troutdale Airport, and for SATURN 06 from the Portland International Airport, as no wind speed sensors are deployed nearby the Morrison Bridge site. USGS water velocity data for the Willamette were recorded at SATURN 06, whereas velocity measurements for the SATURN 08 site were obtained from the downstream USGS 14144700 sensor in nearby Vancouver WA.

3.2 Sample-based measurements

3.2.1 Sampling protocol

We began field sampling in July 2017. The site chosen for the Columbia River was on the dock at the Port of Camas-Washougal marina, in close proximity to the SATURN 08 sensor. Water column depth at that site ranges throughout the year from 7 meters in the summer to 12 meters during the spring freshet. The initial site chosen for the Willamette was located on the waterfront adjacent to the lower terminal of the Portland Ariel Tram and just south of the Ross Island Bridge. However, this site did not afford access to a dock above a water column sufficiently deep to sample at multiple depths and measure light profiles, so activity was limited to shore-based surface sampling. Starting in November 2017, this site was moved south to a dock at Willamette Park, located on the west bank of the river at roughly the same latitude as the southern tip of Ross Island. While the water column here was relatively shallow (from 3 meters in summer to 6 meters in winter), it was sufficient to allow light measurements and multiple depth sampling. It was assumed that the distance of this site upriver of the SATURN 06 sensor (approximately 4.5 kilometers) would be negligible for river primary production measurements. The two sites were each sampled weekly, on two successive days. Whenever possible, the Columbia site was sampled on Wednesdays and the Willamette site was sampled on Thursdays, to maximize regular temporal spacing.

3.2.2 BOD bottle incubations

We took water samples weekly at both sites and at two different depths, within 2 hours of noon. Triplicate surface samples were taken with 1 L opaque Nalgene bottles, both for measurement of oxygen dynamics and for chlorophyll determination. Opaque bottles were necessary to prevent any additional photosynthesis while in transit. The depth of surface grabs is recorded as “0 meters”; however, this is more of a categorical designation, and the actual sampling depth was approximately 10 cm below the surface to avoid contamination by surface films or floating particles. In addition to the three bottles, two additional samples were taken in transparent 500 mL bottles, for nutrient analysis.

The second sampling depth was targeted as the limit of the photic zone, estimated as the depth at which light attenuates to 1% of surface incident light. This was accomplished with a WildCo Van Dorn bottle, a cylindrical sampling trap that snaps shut when struck by a weighted messenger dropped down its rope, similar to a Niskin bottle. A 5 lb (2.27 kg) weight was attached to the Van Dorn bottle to counteract horizontal drag. We used the position of the zip tie marking the length of rope to reach the approximate 1% limit (3.3.1), and let the Van Dorn bottle rest at that depth for approximately 30 seconds, after which the messenger was dropped and the sampler returned to the surface. If the physical bottom of the river was shallower than the 1% light depth, we took samples from just above the bottom instead, raising the Van Dorn bottle approximately 0.5 m after gently touching the benthos, and moving it vertically up and down over a 0.5 m vertical range for 30 seconds to flush out any sediment accumulated on contact. Three casts with the Van Dorn were taken, to fill three more opaque 1 L Nalgene bottles and two more transparent 500 mL nutrient bottles.

All bottles from both depths, upon being filled, were placed in a backpack with several ice packs. Upon returning to our vehicle, we placed them in a cooler with more ice packs for transport back to the laboratory. Once returned, samples were placed in a cold room kept at approximately 9°C before being measured. The return trip to the laboratory from Camas took 30-40 minutes, and the return trip from Willamette Park took approximately 10 minutes. Each BOD sample was taken out of the cold room only for measurement, and then returned to the cold room. This process ensured that water samples were never allowed to equilibrate with ambient laboratory temperature (20°C), thus minimizing any temperature-dependent biological activity that might occur before measurements took place.

Each opaque Nalgene bottle was divided into two treatments: “light” and “dark”. These groups were measured within 20 minutes of each other, to ensure reliable comparisons. The overall goal was to compare the hourly rate of NPP of a sample when exposed to light, to its hourly rate of ER when kept in darkness. Adding the NPP to the absolute value of ER would yield an estimate of hourly GPP. With both depths being sampled in triplicate and each individual sample being divided into two different

treatment groups, this made for a total of 12 BOD bottles used on each sampling day. This meant there was a “light/surface” group, a “dark/surface” group, a “light/deep” group and a “dark/deep” group, each with three replicates.

BOD measurements were made following USGS protocol (Delzer & McKenzie 2003), with one exception regarding temperature equilibration, as noted below. Dissolved oxygen was measured using a YSI OBOD (Optical Biochemical Oxygen Demand) 626401 probe. Prior to measuring, each sample was poured into a 300 mL Wheaton glass BOD bottle. The probe was designed to fit snugly in BOD bottles so that no gas bubbles would be trapped in the neck and thus alter the measurement. The YSI probe logged DO in mg L^{-1} and saturation percentage, as well as temperature and ambient pressure. The probe also included a motorized paddle, to ensure homogeneous circulation during measurement. Values were recorded once the DO concentration was stable. While small fluctuations of the measurement are inherent, we determined that the DO reading was stable when it dropped from its observed maximum value by 0.01 mg L^{-1} and returned to that value at least three times.

After measurement, the probe was rinsed with MilliQ-filtered water and placed in a BOD bottle half full of MilliQ, to keep the probe in 100% water saturated air and thus prevent calibration drift. The sample was immediately sealed with a glass stopper, with care taken to prevent any visible gas bubbles from being trapped. To prevent evaporation of the water seal surrounding the stopper, an over-cap was needed. For this, we wrapped a piece of parafilm tightly around the top of the bottle. The sample was then placed in a cold room kept at 15°C on a shaker table running at 85 rpm to prevent settling. The “light/surface” samples were exposed to a full spectrum lamp, at a power level and distance that set their exposure at approximately $260 \mu\text{E m}^{-2} \text{ s}^{-1}$. To simulate light levels experienced at the lower limit of the euphotic zone, the “light/deep” BOD bottles were wrapped in enough layers of neutral density screening to approximate 1% of the intensity experienced by the “light/surface” bottles, or about $2.6 \mu\text{mol photons m}^{-2} \text{ s}^{-1}$. The two “dark” groups, both surface and deep, were placed under a shroud comprised of two doubled-up black garbage bags, the aperture of which was weighted down with a bungee cord, to prevent

contamination with ambient light. The shaker table beneath these bottles was also covered with two layers of garbage bag material.

After 4 hours \pm 20 minutes, the samples were removed one by one from the cold room for a second measurement with the probe, in the same order they were incubated. The change in dissolved oxygen was divided by 4 to get the approximate hourly rates of production and respiration. While production and respiration rates are not expected to remain constant within a sealed sample, it was assumed that within the short time frame described here this would be an appropriate average. Because temperatures in the actual river were usually greater or less than 15°C depending on the time of year, we adjusted measured respiration rates with an assumed Q_{10} value of 2.2 (Apple et al. 2006).

The light exposed samples were removed for disposal and cleaning, while the dark samples were sealed and returned to the shaker table. They were measured again after 5 days \pm 4 hours, to find their BOD₅ value, a standard measurement of total biochemical oxygen demand. However, because the protocol referred to here (Delzer & McKenzie 2003) demands that samples be equilibrated to 20°C before any measurements are taken, and then maintained at that temperature, BOD₅ values listed here should be used with caution when comparing them with the results of other studies.

After sample disposal, bottles and stoppers were left to soak in a warm solution of tap water and LiquiNox for at least 60 minutes. These were then triple rinsed with deionized water and submerged in a solution of 10% hydrochloric acid for at least 60 minutes. Afterward, they were triple rinsed with MilliQ and left to air dry overnight.

3.2.3 Chlorophyll

The triplicate BOD samples (3.2.1) were also used for chlorophyll *a* extraction. 200 mL of each of the three replicates was passed through a 0.7 μ m glass fiber filter, using a vacuum filter manifold. If water samples were visibly turbid, 100 mL was used instead to avoid clogging of the filter. Following a non-acidified chlorophyll extraction protocol (Welschmeyer 1994), these filters were frozen at -20°C until

needed for extraction, whereupon they were each placed in 8 mL 90% acetone solution in a disposable glass culture tube, and returned to the freezer for 24 hours (± 2 hours). These samples were measured approximate 25-30 at a time, with each run including three 90% acetone blanks. The filters were then discarded, and the supernatant from each was poured into a cuvette tube. The Raw Fluorescence Units (RFU) of each sample were then measured using a Turner Trilogy fluorometer with a chlorophyll *a* non-acidified module. Correcting this value with the average of the blanks, we calculated the concentration of chlorophyll in each sample in $\mu\text{g L}^{-1}$ (Welschmeyer 1994).

3.2.4 Inorganic nutrients

Nutrients were sampled as duplicate whole water grabs from both optical depths, in transparent plastic sampling bottles. These samples were passed through a 0.7 μm glass filter and frozen at -20°C until ready for analysis, at which point they were left to thaw in a 55°C water bath. Nutrients measured included nitrate, nitrite, ammonium and ortho-phosphate using an Astoria-Pacific Analyzer and accepted colorimetric or fluorometric protocols (Armstrong et al. 1967, APHA 1992, Holmes et al. 1990), and the duplicate samples were averaged. The mean for each DIN timepoint at each depth was then divided by the mean DIP, to assess relative nutrient limitation relative to the 16:1 Redfield ratio.

3.3 Field measurements

3.3.1 CTD Casts and Light Attenuation

Upon arrival at a site, the field equipment was assembled. This consisted of a LiCor LI-1500 light sensor attached to a SonTek CastAway CTD (conductivity, temperature, depth). This was lowered for three casts to measure light availability throughout the water column. First, the instrument was suspended just below the water's surface for 30 seconds, to allow stabilization of the signals. Because the light sphere and the CTD were two separate instruments, the assembly was lowered in a "stepwise" fashion, stopping at two more depths at least 1m apart in the Columbia, or 0.5 m apart in the Willamette due to the shallower depth at the site. This would allow easier correlation of the two datasets by creating a

recognizable pattern. Comparing the light recorded at depth to the reading from an attached terrestrial light sensor allowed estimation of the approximate 1% light depth, at which point the sensor was allowed to rest for an additional 30 seconds. It was then lowered until it touched the channel bottom and left for 30 more seconds. After this, it was raised, stopping two more times on the way up. This process was repeated three times. The data for the three casts were binned by depth category, at 1m intervals in the Columbia and 0.5_m intervals in the Willamette. By normalizing the recorded underwater light at each depth interval to the average surface incident light, variations in surface light could be removed from the light data. The three casts were then averaged with each other to produce a modeled light decay curve for that site and day. This simple exponential decay function allowed calculation of the 1% light depth.

3.3.2 Water column stratification

In addition to logging the depth, the CTD recorded salinity and temperature. Using the data from the light casts, we could use these measurements to quantify the degree of stratification between the surface and the bottom. Data from the top and bottom meters of the water column at Camas – or the top and bottom 0.5 meters at the Willamette site – were placed in “surface” and “deep” bins. This allowed us to obtain the difference between the top and bottom of the water column for each quantity.

At the Columbia site, we deployed an additional sonde sensor for a single cast for 15 weeks in spring through summer 2018, to measure DO concentrations and saturation along the water column. The sensor used a similar optical probe to the YSI employed in BOD dissolved oxygen measurements (3.2.2). The probe was suspended just below the surface until the reading appeared to stabilize, after which it was lowered slowly until reaching the channel bottom. It was left at the bottom for 30 seconds, slowly returned to the surface, and left for an additional 30 seconds at the surface. This was done to test whether dissolved oxygen varies significantly through the water column. DO concentration and saturation data were binned and analyzed in the same way as temperature and conductivity.

4.0 Results

4.1 GPP and ER

Sensor-based estimates of GPP and ER largely followed expected trends in the Columbia (Figure 2.2a), with GPP exceeding respiration most of the year and a large phytoplankton bloom occurring between March and May, but with peaks in GPP being almost matched by large spikes in ER. Although a large gap exists because the sensor was removed for maintenance between October and February, trends on either side of the gap implied low rates of production and respiration through the winter, with a decline in late August 2017 and an increase starting in early spring. The Willamette had significantly lower biological activity throughout most of the year, appearing slightly autotrophic – except for late summer, when large peaks of GPP were exceeded by even larger peaks of ER (Figure 2.2b). These peaks corresponded with the nearby cyanobacteria bloom observed in the Ross Island Lagoon, as well as elevated temperatures (Figure 2.6), and lower flow which may have increased water residence times (Figure 1.2).

To test the sensitivity of our gas diffusion estimates and their impact on our open-water respiration signal, we performed sensitivity analysis of various wind speeds on the wind-induced diffusion flux rate (k_{wind} , in cm h^{-1}) (Figure 2.1a), and on the effect of different current velocities on the turbulence-induced diffusion flux rate (k_{flow} , in cm h^{-1}) (Figure 2.1b). K_{wind} showed a relationship similar to those seen in lakes – as described by Wanninkhof (1992) – with increasing sensitivity at higher wind velocities. K_{flow} showed a diminishing sensitivity at higher current velocities.

Because the depth of the water column below the sensor was needed, both for the calculation of diffusion caused by flow and for conversion from areal NEM rates to volumetric, we assumed a water column depth in both rivers of 7m, which is close to the average for the Columbia site and close to the approximate bathymetric profile in the Willamette mid-channel in downtown Portland. To test the impact that the accuracy of this depth figure had on our results, we compared calculations of respiration with and

without the k_{flow} term, as well as various simulated current velocities, finding a negligible difference at the velocities encountered during the study period (Figure 2.1d).

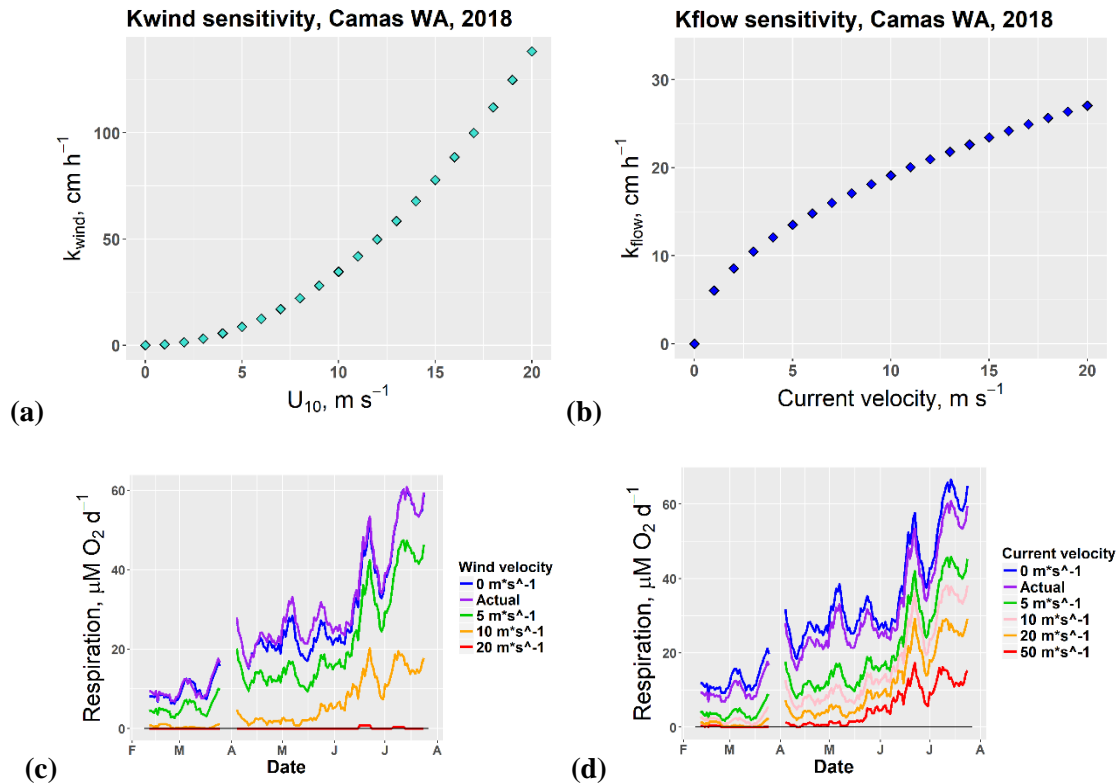


Figure 2.1: (a) Comparison of estimates of ER in the Columbia River with the wind velocity variable set at various values, where U_{10} is the wind velocity 10 meters above the water surface. (b) Comparison of estimates of ER in the Columbia River with the current velocity variable set at various values, where U_{10} is the wind velocity 10 meters above the water surface. (c) Estimates of respiration in the Columbia River at different wind speeds, including those observed during the study period. (d) Estimates of respiration in the Columbia River at different current velocities, including those observed during the study period.

BOD-based estimates of GPP in the Columbia were similar to sensor-based estimates, showing a weak ($R^2 = 0.47$) but significant relationship (Figure 2.3a). GPP was not calculated with BOD samples prior to winter 2017 because light incubations were not yet being conducted – hence, gaps in the data exist for the first part of the timeseries (Figure 2.2c). In the Willamette, patterns in GPP mostly corresponded between the two estimates, showing low activity for most of the year and a substantial peak in late July, matching the spike recorded by the sensor during the late summer cyanobacteria bloom the previous summer

(Figure 2.2d). The relationship between the two estimates was weaker than in the Columbia ($R^2 = 0.23$) but still significant (Figure 2.3b) and had a slope close to 1. BOD dark bottle hourly ER estimates did not closely match the sensor estimates for either river. In both cases, the recorded hourly metabolism was significantly lower than that estimated by the sensors based on night respiration, with the Columbia having the most pronounced difference. At its most extreme, during the peak of the phytoplankton bloom in early summer 2018, the sensor-based estimate of ER was roughly similar in magnitude to the recorded GPP – and even as the GPP estimate from the BOD experiments closely matched the sensor, the ER rates were smaller than the sensor estimates by more than tenfold. The only exception to this trend was a large spike in production and respiration in the Willamette in February (Figure 2.2d), which corresponded with a major flux event in the river (Figure 1.2). This particular measurement may be spurious, however, because a similar spike was not recorded in the deep BOD sample (Figure 2.2f). The deep samples showed little difference between each other, with very low rates of both production and respiration.

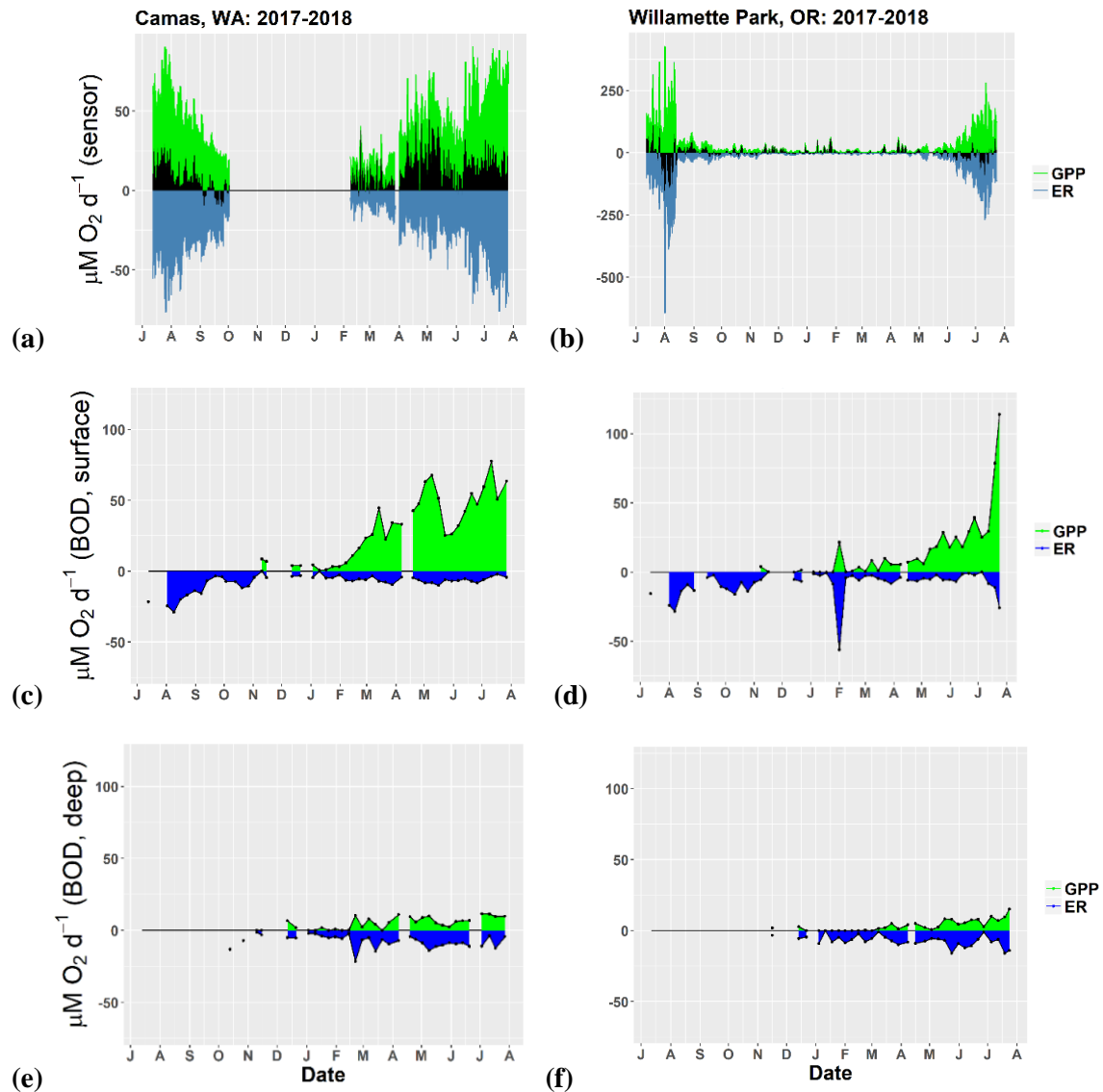


Figure 2.2: Comparison of NEM, GPP, and ER for the Columbia and Willamette rivers. **(a)** 7-day moving average of daily GPP, NEM, and ER for the Columbia River at Camas-Washougal WA, calculated using data from the SATURN 08 sensor. **(b)** 7-day moving average of daily GPP, NEM, and ER for the Willamette River at Willamette Park OR, calculated using data from the SATURN 06 sensor. Note that the y-axis scale on this figure differs from the others. **(c)** Weekly estimate of surface daily GPP and ER for the Columbia River at Camas-Washougal WA, calculated using BOD bottle incubations. **(d)** Weekly estimate of surface daily GPP and ER for the Columbia River at Camas-Washougal WA, calculated using BOD bottle incubations. **(e)** Weekly estimate of deep daily GPP and ER for the Columbia River at Camas-Washougal WA, calculated using BOD bottle incubations. **(f)** Weekly estimate of deep daily GPP and ER for the Columbia River at Camas-Washougal WA, calculated using BOD bottle incubations.

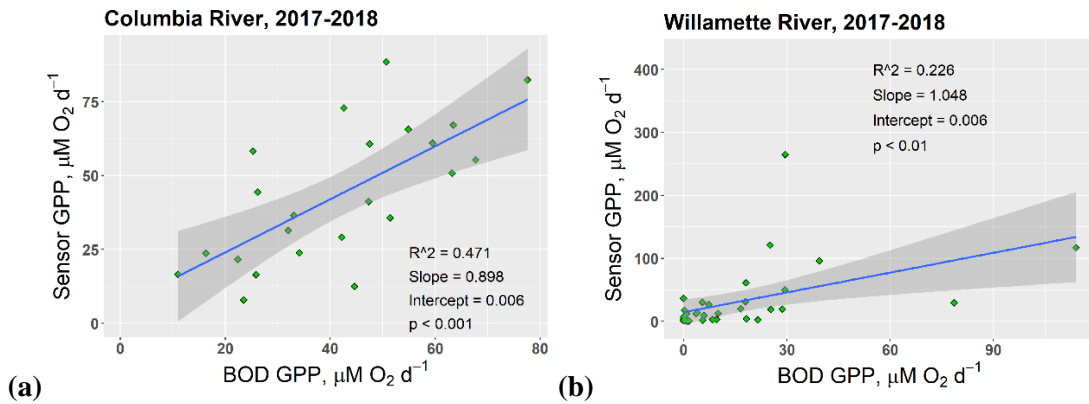


Figure 2.3: (a) Regression analysis of sensor-based and BOD incubation-based measurements of gross primary production in the Columbia River. (b) Regression analysis of sensor-based and BOD incubation-based measurements of gross primary production in the Willamette River.

To determine the reliability of our hourly BOD respiration rates, we compared them to the BOD₅ values, with the assumption that the very small recorded values of hourly respiration might be noisy, and the larger BOD₅ values more stable (Figure 2.4). We found that, while this was the case, both values followed a similar pattern, with the BOD₅ measurements being consistently larger than the hourly ER values by a factor of approximately 3. Because the 1-hour estimates were obtained as an average of the 4-hour timepoint measurements, this means that around a third of the 5 day change in oxygen in the sample takes place in the first 4 hours of incubation. The pattern in the BOD₅ data in both rivers appears to closely match the patterns of GPP (Figure 2.2) and chlorophyll *a* (Figure 2.8). BOD₅ rates in the Columbia also showed a weak correlation with dissolved organic matter (DOM) measured by the sensor (Figure 2.5a), and a weak correlation during the summer in the Willamette that became completely decoupled during fall through spring (Figure 2.5b). This suggests that DOM controls respiration in the Columbia because it is more labile, due to being sourced primarily from phytoplankton biomass, whereas DOM in the Willamette comes mainly from runoff during discharge peaks and storms (Figure 1.2), which are also correlated with spikes in turbidity (Figure 2.6d).

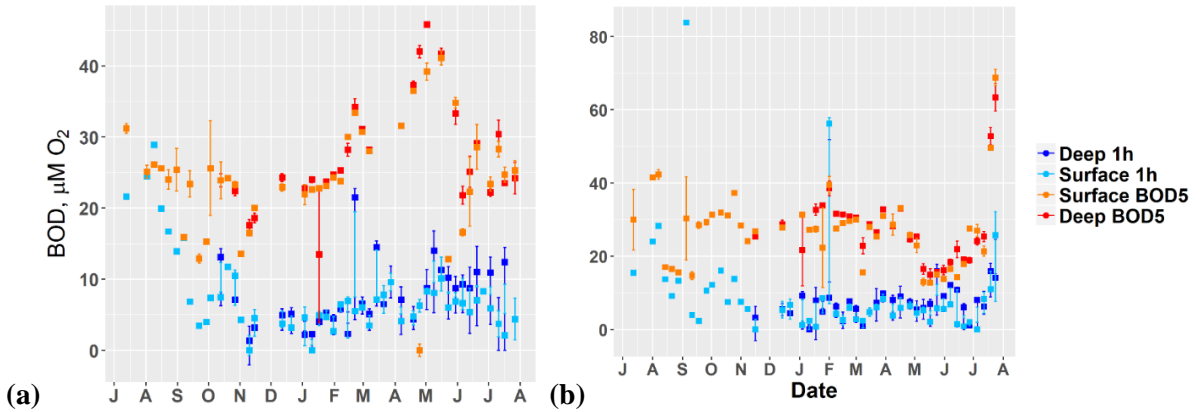


Figure 2.4: (a) Comparison of 5-day dark respiration at two sample depths in the Columbia River with 1-hour dark bottle respiration. (b) Comparison of 5-day dark respiration at two sample depths in the Willamette River with 1-hour dark bottle respiration.

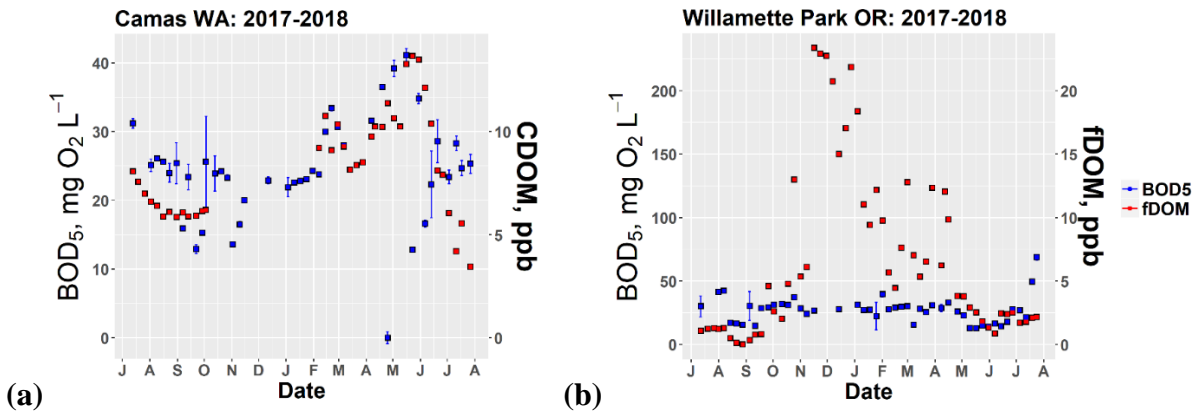


Figure 2.5: (a) Comparison of 5-day dark respiration and dissolved organic matter in the Columbia. (b) Comparison of 5-day dark respiration and dissolved organic matter in the Willamette.

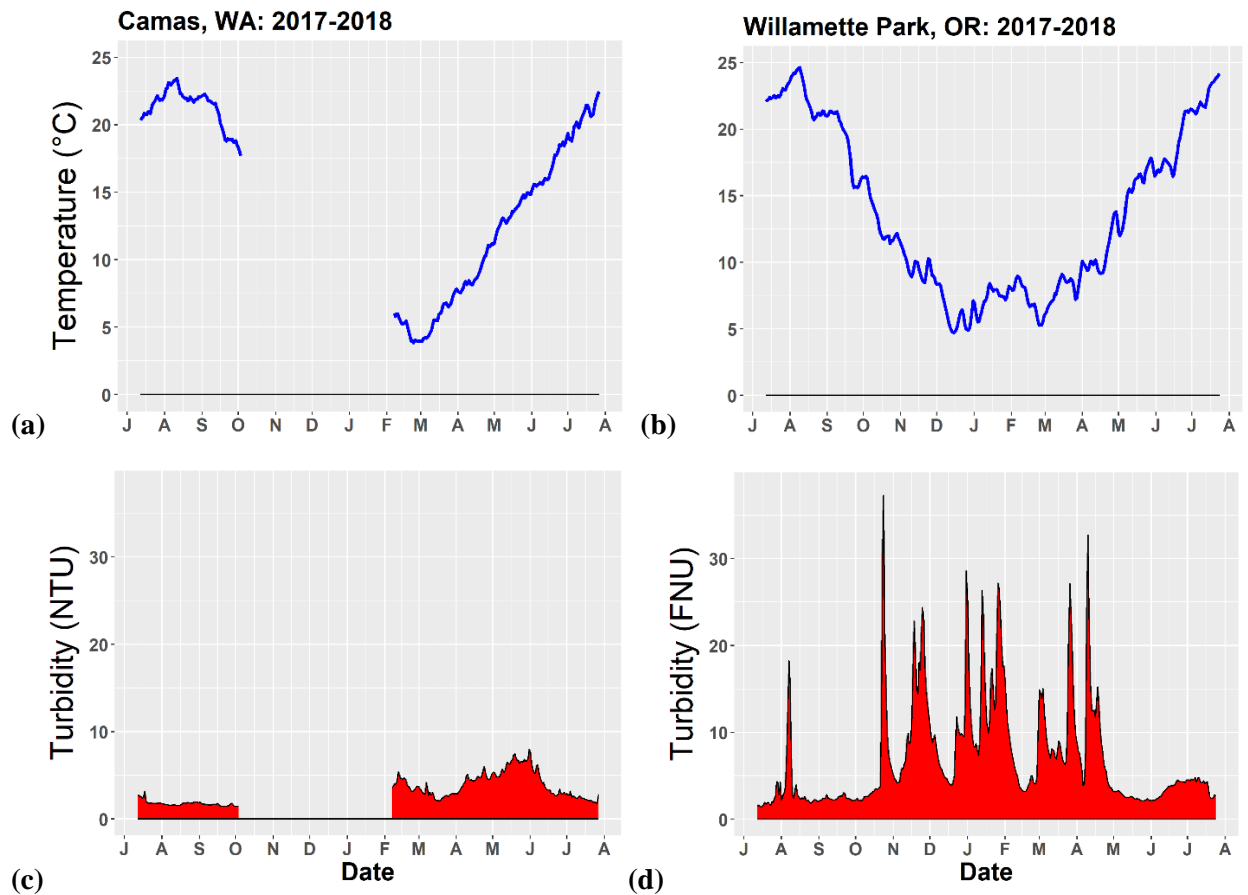


Figure 2.6: (a) Water temperature in the Columbia. (b) Water temperature in the Willamette River. (c) Turbidity in the Columbia, reported in nephelometric turbidity units (NTU). (d) Turbidity in the Willamette, reported in formazin nephelometric units (FNU).

4.2 Chlorophyll and particulate organic carbon

Sample measurements of chlorophyll (Figure 2.8a, b) closely followed the patterns detected by the sensor but were scaled differently, due to different reference standards. To correct the sensor readings based on our samples, we did regression analyses comparing the sensor reading to both the surface and deep sample groups, averaging the coefficients between groups to obtain a function to apply to the sensor outputs (Figure 2.7). We obtained average slopes of 2.99 and 2.17, and intercepts of 1.11 and 0.74 for the Columbia and Willamette, respectively.

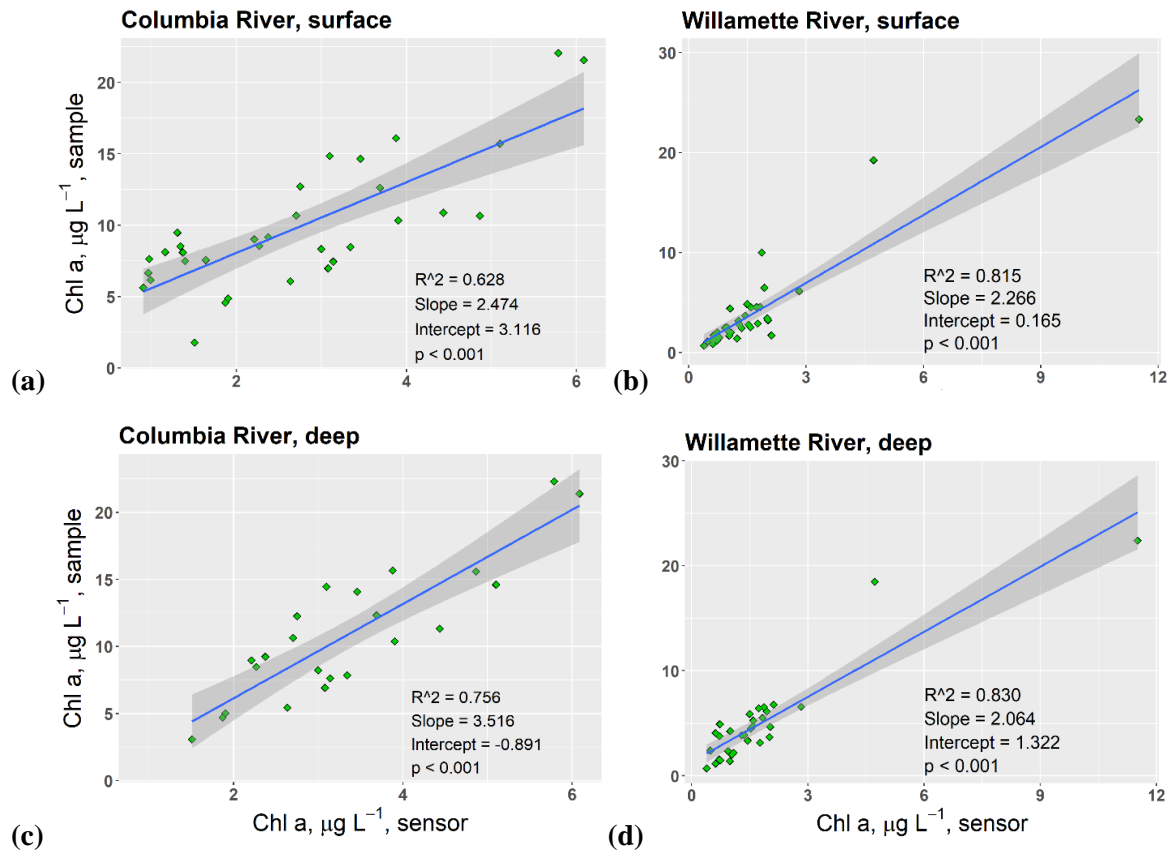


Figure 2.7: (a) Regression analysis of surface sample measurements of chlorophyll *a* and sensor-based measurements, Camas WA 2017-2018. (b) Regression analysis of surface sample measurements of chlorophyll *a* and sensor-based measurements, Willamette Park OR 2017-2018. (c) Regression analysis of deep sample measurements of chlorophyll *a* and sensor-based measurements, Camas WA 2017-2018. (d) Regression analysis of deep sample measurements of chlorophyll *a* and sensor-based measurements, Willamette Park OR 2017-2018.

Chlorophyll *a* concentrations in the Columbia appeared to follow a pattern similar to total GPP (Figure 2.2a), peaking in May and remaining relatively high through the summer (Figure 2.8c). This pattern is consistent with the observations of a seasonal spring bloom. The Willamette showed generally lower concentrations, but with some large peaks in the summer as well (Figure 2.8d). The sample measurements showed that chlorophyll *a* did not differ significantly between depths in either river (Figure 2.8a, b, 2.9).

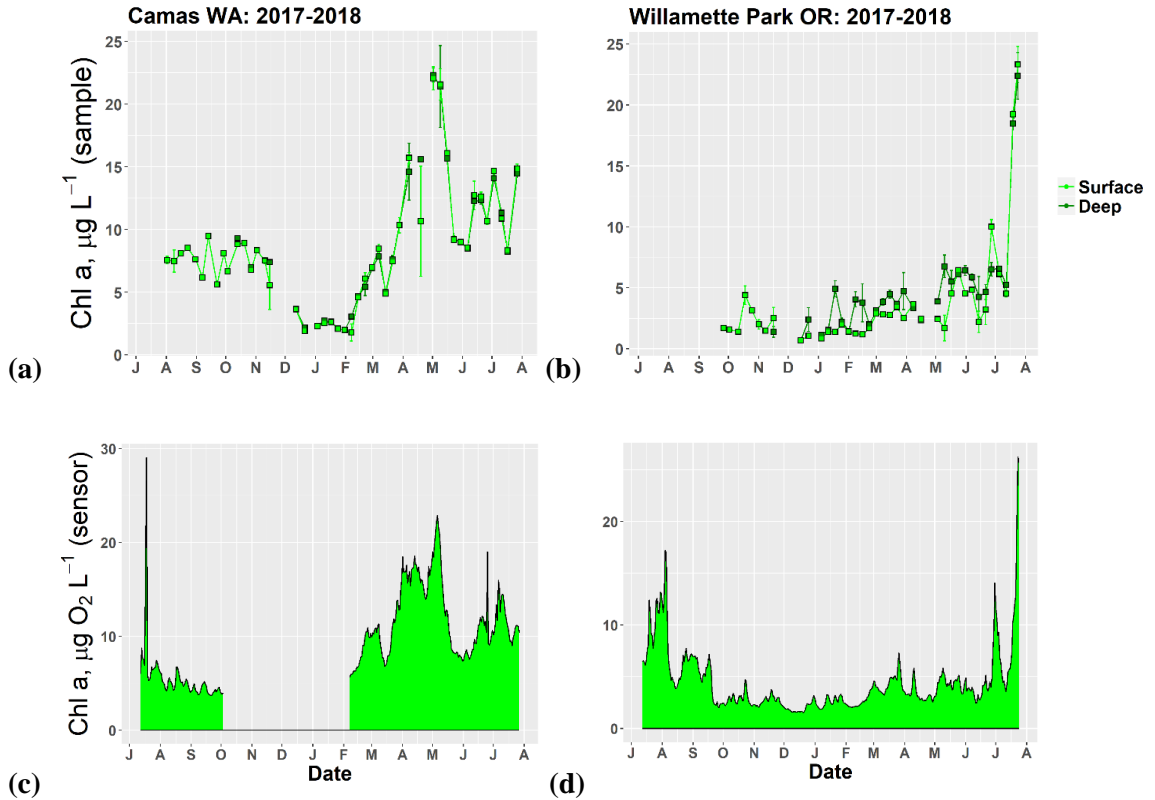


Figure 2.8: (a) Chlorophyll *a* concentration at two different depths in the Columbia River at Camas-Washougal WA, based on sample measurements. (b) Chlorophyll *a* concentration at two different depths in the Willamette River at Willamette Park OR, based on sample measurements. (c) Timeseries of daily average chlorophyll *a* in the Columbia, downloaded from the SATURN-08 sensor and adjusted based on the results of the sample regression analysis (Figure 2.3). (d) Timeseries of daily average chlorophyll *a* in the Willamette, downloaded from the SATURN-08 sensor and adjusted based on the results of the sample regression analysis (Figure 2.3).

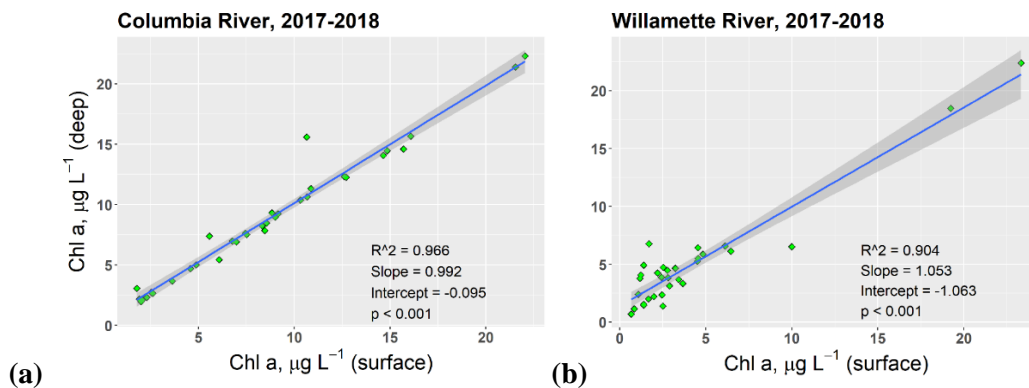


Figure 2.9: (a) Regression analysis of chlorophyll *a* concentrations between depths at Camas WA. (b) Regression analysis of chlorophyll *a* concentrations between depths at Willamette Park OR.

Assuming a C:Chl mass ratio of 25:1 (Gilbert et al. 2013), we calculated the biomass of phytoplankton standing stock as *particulate organic carbon* (POC), allowing us to compare this with NEM, which was converted from our sensor measurements, assuming a C:O₂ ratio of 106:138 (Redfield 1958).

NEM and phytoplankton biomass followed similar patterns, although the maximum peak for phytoplankton biomass and NEM in the Columbia both peaked in May (Figure 2.10a), with a local minimum in June and a second peak in July. In the Willamette, phytoplankton biomass remained comparatively low throughout most of the year (Figure 2.10b), with peaks in the summer that were far exceeded by NEM.

By converting NEM and ER to POC using a C:Chl mass ratio of 25:1 (Maier & Peterson 2014) and multiplying these values by river discharge, we obtained the total daily carbon flux in both rivers (Figure 2.10c, d). This revealed the Columbia to be a net POC exporter during the majority of the period of sensor deployment, while the Willamette displayed intermittent spikes of POC import and export.

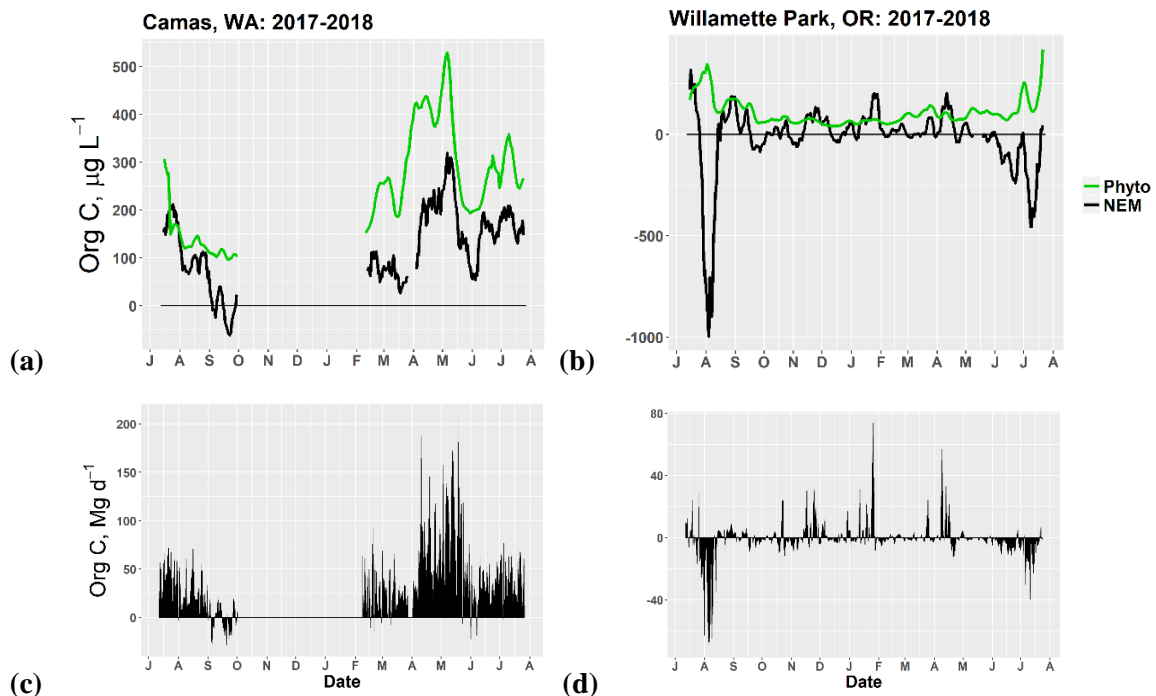


Figure 2.10 (previous page): (a) Comparison of NEM in the Columbia, measured in organic carbon, to POC contained in phytoplankton standing stock, using an estimated C:Chl ratio of 25:1. (b) Comparison of NEM in the Willamette, measured in organic carbon, to POC contained in phytoplankton standing stock, using an estimated C:Chl ratio of 25:1. (c) Total daily organic carbon flux in the Columbia. (d) Total daily organic carbon flux in the Willamette.

4.3 Inorganic Nutrients

The sensor and sample measurements of nitrate in both rivers followed similar patterns, with a slight but consistent difference between the samples and sensor measurements (Figure 2.11). To correct the sensor data, we did regression analyses to compare the sensor readings to both depth groups (Figure 2.12), and averaged the coefficients to yield a single correction for each river. We obtained slopes of 0.91 and 0.83, and intercepts of -1.88 and -1.11 for the Columbia and Willamette, respectively.

Nitrate in both the Columbia and the Willamette followed similar patterns (Figure 2.11a, b) with a peak in winter and significant declines through spring, corresponding with the plankton bloom. Phosphate in the Columbia diminished in the spring following a similar pattern to nitrate (Figure 2.11c). In the Willamette, it showed no apparent trend (Figure 2.11d). In both rivers, no significant difference between depths was observed, and total concentrations were consistently higher in the Willamette than the Columbia. N:P ratios in both rivers showed an overall drop during the spring (Figure 2.11e, f), indicating that nitrogen was likely used up at a faster rate than phosphorus during the spring blooms. The few data points available in fall 2017 suggest that N:P was low during that period, even reaching or dropping below the Redfield ratio.

Regression analysis of nitrate revealed no difference between depths in either river (Figure 2.13a, b) and a significant but weak relationship between phosphate (Figure 2.13c, d), indicating the possibility that phosphate concentrations variable but higher near the surface in both rivers.

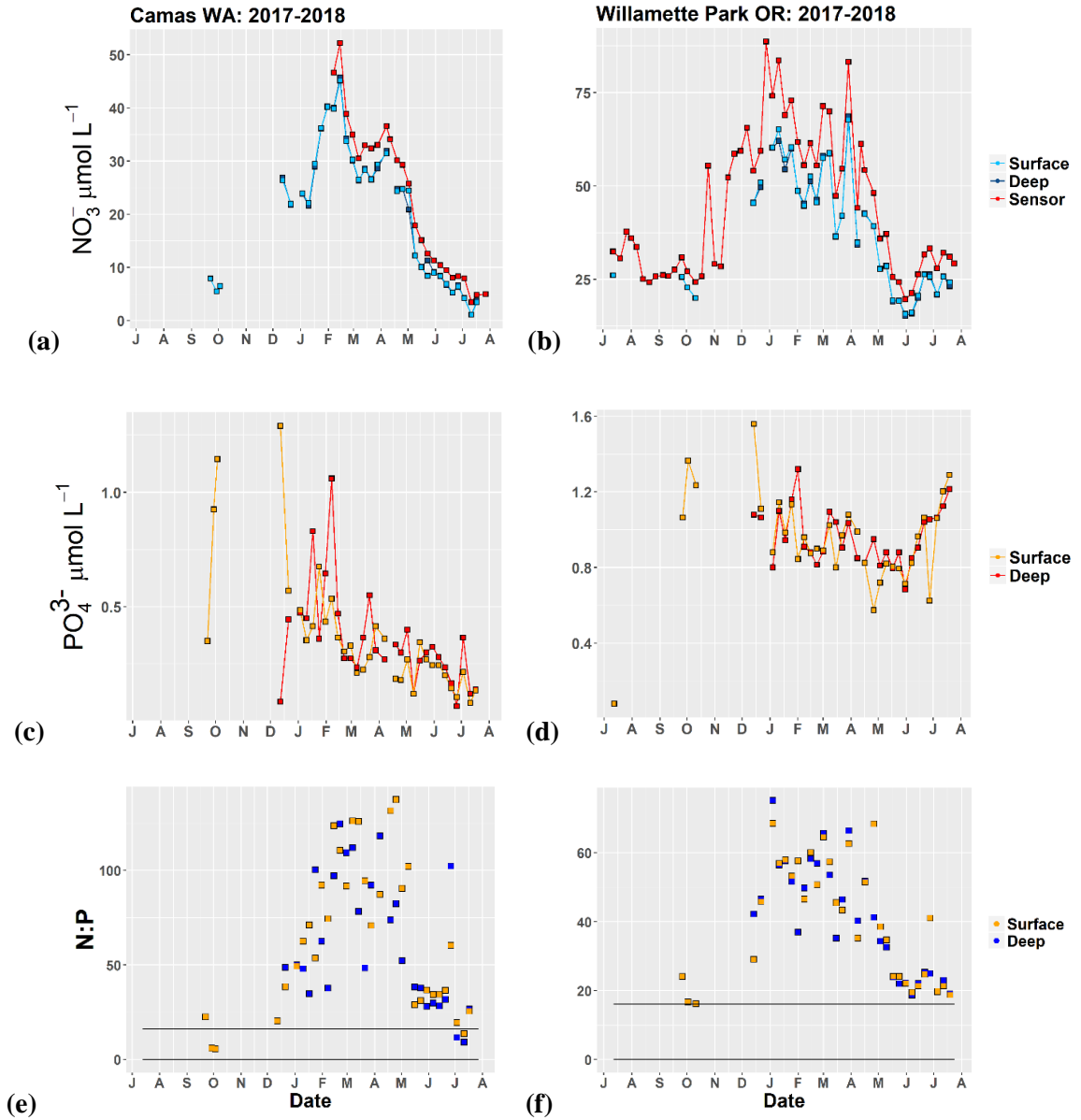


Figure 2.11 (previous page): (a) Nitrate concentrations in the Columbia River at Camas-Washougal WA, sampled at two different depths, with sensor measurements. (b) Nitrate concentrations in the Willamette River at Willamette Park OR, sampled at two different depths, with sensor measurements. (c) Phosphate concentrations in the Columbia River at Camas-Washougal, WA, sampled at two different depths. (d) Phosphate concentrations in the Willamette River at Willamette Park OR, sampled at two different depths. (e)

N:P ratio in the Columbia, with a horizontal line corresponding to the Redfield Ratio of 16:1. **(f)** N:P ratio in the Willamette, with a horizontal line corresponding to the Redfield Ratio of 16:1.

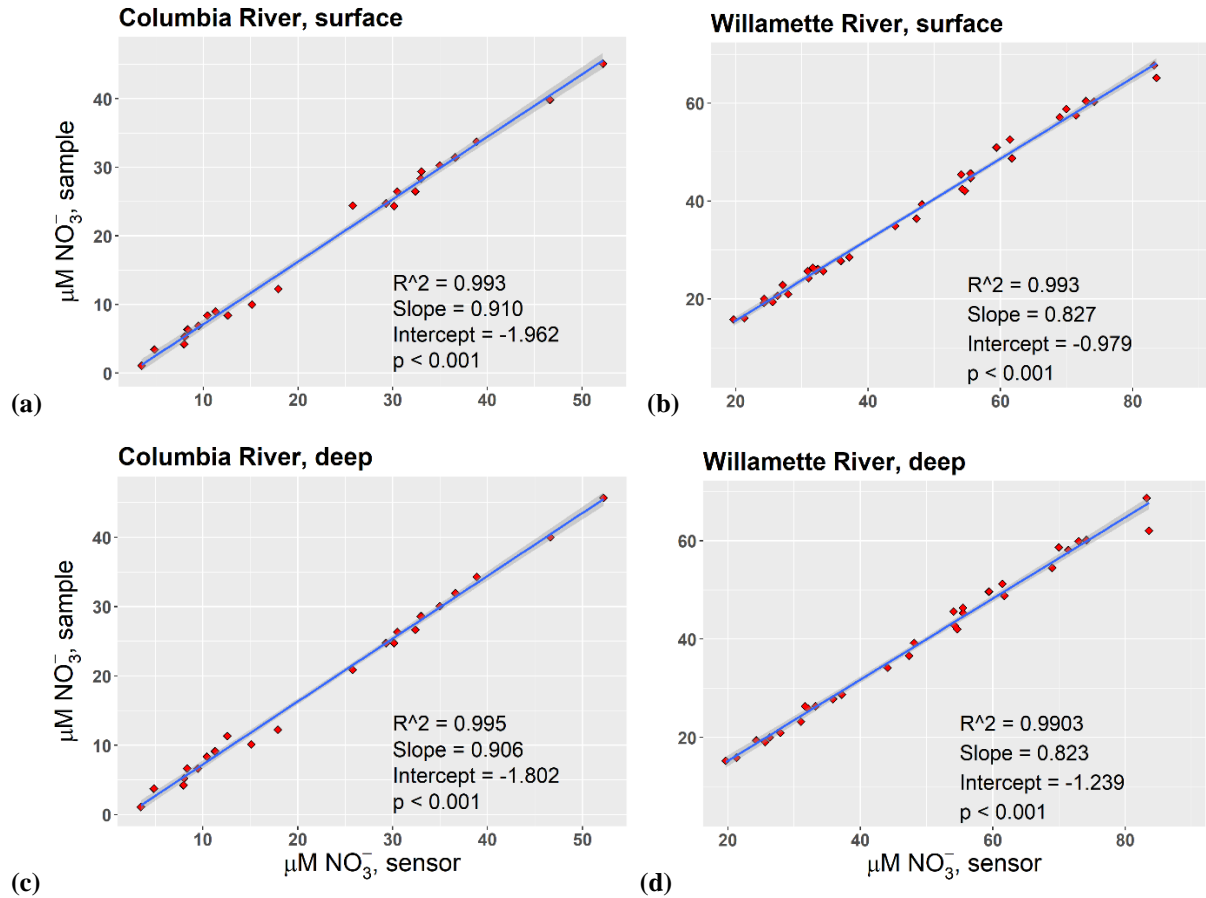


Figure 2.12: **(a)** Regression analysis of surface sample and sensor-based measurements of nitrate, Camas WA 2017-2018. **(b)** Regression analysis of surface sample and sensor-based measurements of nitrate, Willamette Park OR 2017-2018. **(c)** Regression analysis of deep sample and sensor-based measurements of nitrate, Camas WA 2017-2018. **(d)** Regression analysis of deep sample and sensor-based measurements of nitrate, Willamette Park OR 2017-2018.

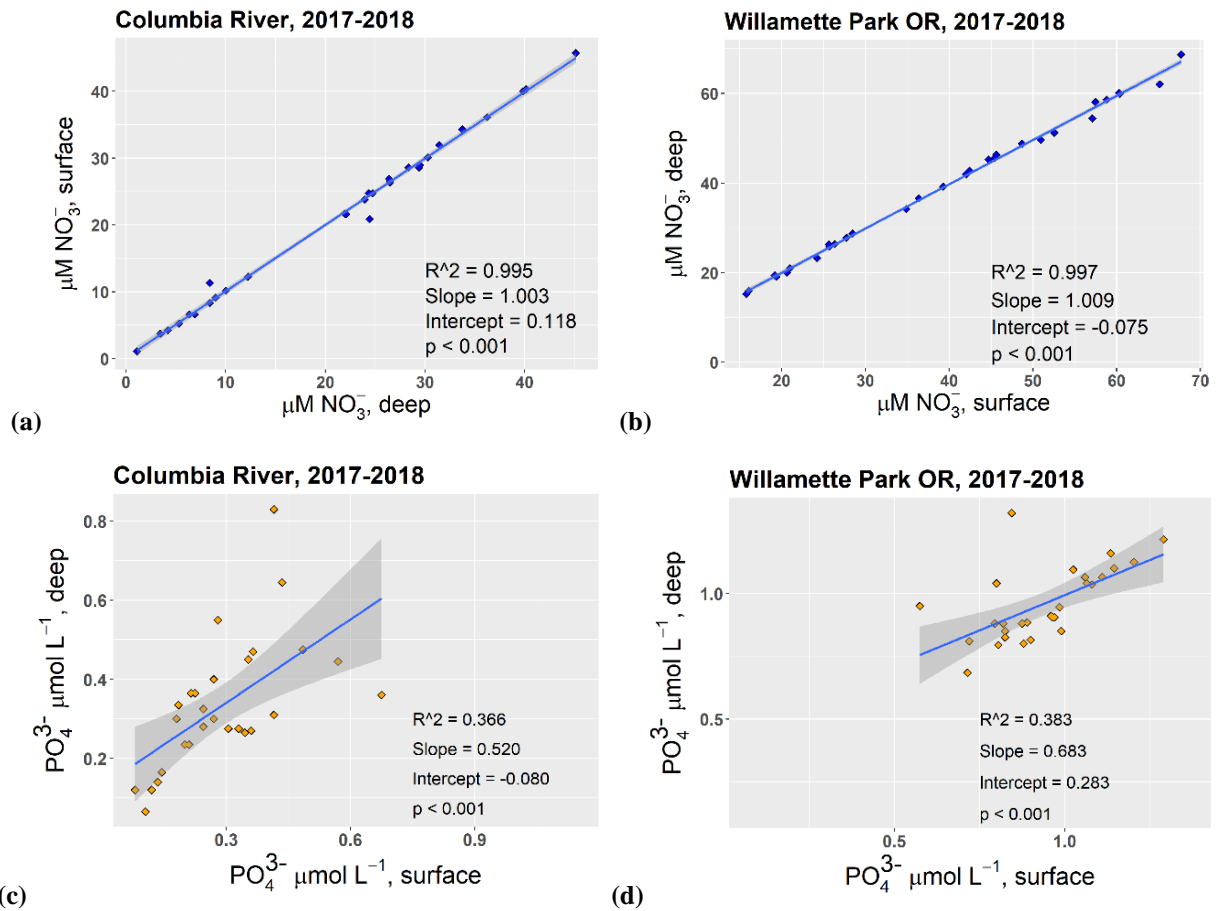


Figure 2.13: (a) Regression analysis of nitrate between depths in the Columbia, 2017-2018. (b) Regression analysis of nitrate between depths in the Willamette, 2017-2018. (c) Regression analysis of phosphate between depths in the Columbia, 2017-2018. (d) Regression analysis of phosphate between depths in the Willamette, 2017-2018.

To further explore the possibility of N-limitation, we compared organic carbon in phytoplankton biomass in $\mu\text{M N}$, assuming a C:N ratio of 106:16, to Dissolved Inorganic Nitrogen (DIN). Data for the Columbia were only available from February 2018 on, but showed rapid drawdown through spring and summer (Figure 2.14a). We compared the rate of DIN drawdown with NEM, also converted from carbon to μM organic N. The steepest declines in DIN in the Columbia during the spring corresponded with the highest rates of NEM (Figure 2.14c). NEM and phytoplankton biomass began to drop after DIN

concentrations dropped below NEM. This corresponded with points when the N:P ratio was close to or below the Redfield ratio (Figure 2.11e). In the Willamette, DIN far exceeded phytoplankton N (Figure 2.14b), with peaks of nearly 80 μM , and dropping to around 20 μM in the summer. During the periods of strong heterotrophy, slight peaks of DIN rose inversely to drops in NEM, showing that the high rates of aerobic respiration might be causing remineralization of DIN. By subtracting the DIN drawdown rate from NEM (Figure 2.14c, d), we could calculate the rate of influx of N into the rivers (Figure 2.14e, f).

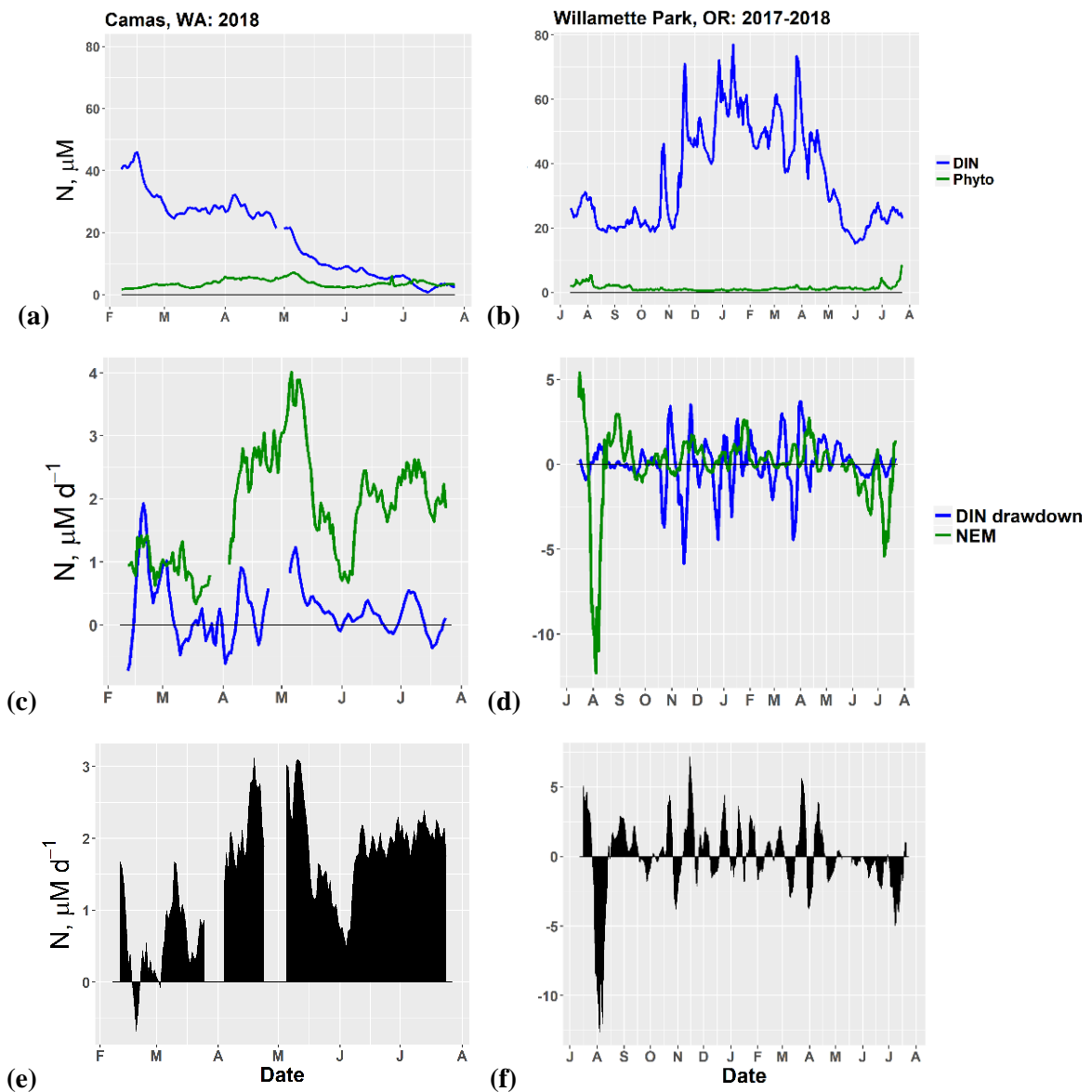


Figure 2.14 (previous page): (a) Dissolved inorganic nitrogen (as nitrate) molar concentration in the Columbia, February-August 2018, compared with organic nitrogen concentration in phytoplankton standing stock, assuming a C:N ratio of 106:16. (b) Dissolved inorganic nitrogen (as nitrate) molar concentration in the Willamette compared with organic nitrogen concentration in phytoplankton standing stock, assuming a C:N ratio of 106:16. (c) Nitrogen NEM at Camas WA, February-August 2018, assuming a C:N ratio of 106:16, compared with daily change in DIN concentration (positive values represent a drawdown of DIN). (d) Nitrogen NEM in the Willamette, assuming a C:N ratio of 106:16, compared with daily change in DIN concentration (positive values represent a net drawdown of DIN). (e) Daily volumetric influx of DIN into the Columbia, February-August 2018. (f) Daily volumetric influx of DIN into the Willamette.

4.4 Field Measurements

The depth of the photic zone was mostly shallower in the Willamette (Figure 2.15), with the exception of May-June, during which the photic zone of the Willamette became deeper and the photic zone of the Columbia became shallower, possibly due to a lack of runoff into the Willamette and attenuation by the phytoplankton bloom in the Columbia.

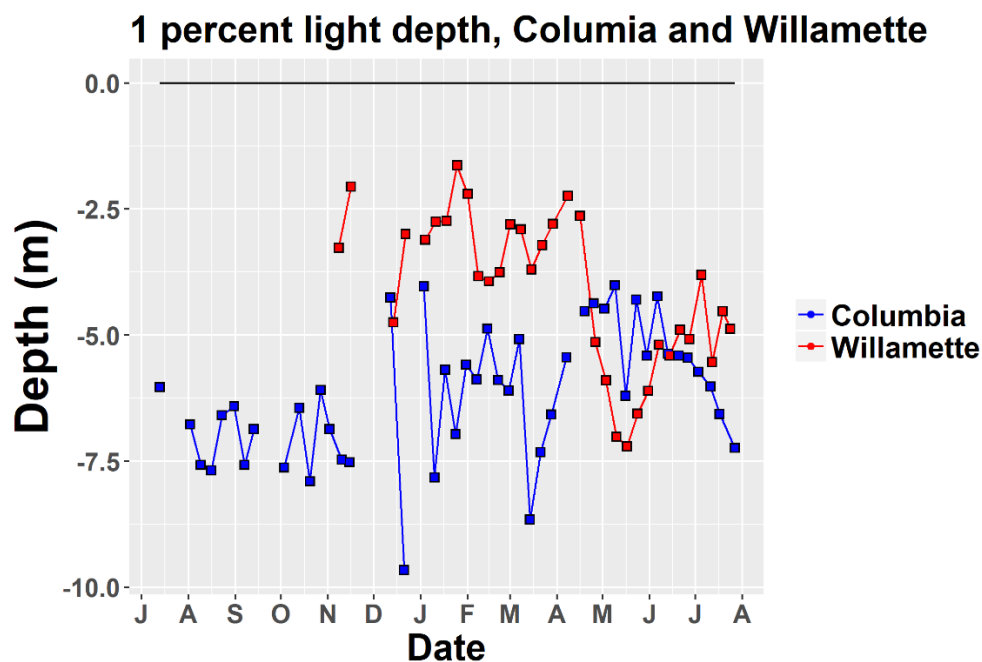


Figure 2.15: Photic zone depth in the Columbia and Willamette rivers, 2017-2018.

The sonde casts for DO during spring 2018 initially showed a steady increase with depth, but this pattern did not repeat during the upward portion of the cast. It was determined that the probe had not been allowed sufficient time to stabilize. To solve this problem, only data from the upward half of the casts were used. The result was no difference between depths (Tables 2.1, 2.2, Figures 2.16, 2.17), with surface and deep measurements never differing by more than a few percent for DO, temperature, and conductivity. For comparison, the temperature and conductivity casts measurements taken in the deep, stratified Ross Island Lagoon had deep temperature and conductivity that varied by 36% and 12%, respectively, from the surface values.

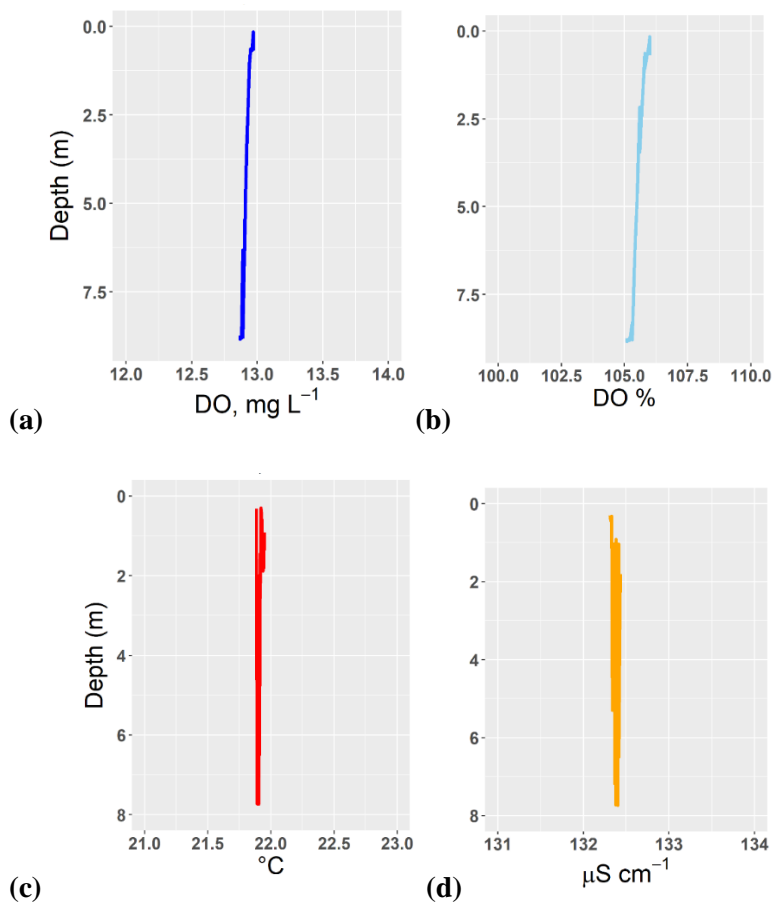


Figure 2.16: Examples of depth profiles in the Columbia River. (a) Water column concentration of DO, March 21st 2018. (b) Water column percent saturation of DO, March 21st 2018. (c) Water column temperature, August 23rd 2017. (d) Water column conductivity, August 23rd 2017.

Date	Water Column Average Value				Surface minus bottom				% change			
	°C	uS cm ⁻¹	DO mg/L	DO %	°C	uS cm ⁻¹	DO mg/L	DO %	°C	uS cm ⁻¹	DO mg/L	DO %
7/13/2017	20.28	108.67			-0.05	-0.23			0.3	0.2		
8/2/2017	22.51	128.05			0.12	0.26			0.5	0.2		
8/9/2017	23.25	133.32			0.15	0.09			0.6	0.1		
8/16/2017	22.16	131.72			0.12	0.32			0.5	0.2		
8/23/2017	21.88	129.24			-0.03	-6.43			0.1	5.2		
8/31/2017	22.13	133.40			0.07	-0.33			0.3	0.2		
9/7/2017	21.94	136.16			0.02	-0.05			0.1	0.0		
9/13/2017	21.29	136.61			0.04	0.09			0.2	0.1		
10/3/2017	17.75	127.63			0.01	-0.58			0.0	0.5		
10/13/2017	15.38	128.32			0.15	0.83			1.0	0.6		
10/20/2017	14.44	123.10			0.02	0.07			0.1	0.1		
10/27/2017	13.39	119.78			0.06	-0.16			0.5	0.1		
11/2/2017	12.95	123.90			0.06	-0.36			0.5	0.3		
11/10/2017	10.66	118.86			0.16	0.65			1.5	0.5		
11/15/2017	10.88	124.95			-0.01	0.01			0.1	0.0		
12/12/2017	6.04	116.85			0.03	-0.28			0.5	0.2		
12/21/2017	6.51	101.24			-0.03	-0.01			0.4	0.0		
1/3/2018	4.36	92.87			-0.06	-0.64			1.5	0.7		
1/10/2018	4.96	93.30			-0.01	-0.52			0.2	0.6		
1/17/2018	5.16	109.90			-0.02	0.03			0.4	0.0		
1/24/2018	5.33	115.62			-0.01	-0.20			0.2	0.2		
1/31/2018	5.59	107.99			0.03	-0.29			0.6	0.3		
2/7/2018	6.16	114.16			0.10	-0.50			1.6	0.4		
2/14/2018	5.41	118.95			0.04	0.10			0.7	0.1		
2/21/2018	4.18	105.45			0.04	-0.28			1.0	0.3		
2/28/2018	4.23	93.04			-0.01	-0.03			0.1	0.0		
3/7/2018	4.50	91.86			-0.02	-0.31			0.4	0.3		
3/14/2018	5.69	97.48			0.07	-0.03			1.2	0.0		
3/21/2018	6.90	104.92	12.92	105.57	0.04	-0.11	0.08	0.73	0.6	0.1	0.7	0.7
3/28/2018	7.36	108.49	12.78	105.90	0.01	-0.12	0.12	1.20	0.1	0.1	0.9	1.1
4/7/2018	8.62	113.66	12.69	108.20	0.01	-1.01	0.09	0.84	0.1	0.9	0.7	0.8
4/19/2018	9.26	123.11	13.47	116.97	0.01	-0.47	0.08	0.77	0.1	0.4	0.6	0.7
4/25/2018	10.71	121.17	12.90	115.94	0.03	-0.06	0.10	0.98	0.3	0.0	0.7	0.8
5/2/2018	11.85	123.47	12.78	117.95	0.05	0.12	0.07	0.72	0.4	0.1	0.6	0.6
5/9/2018	13.28	119.42	12.78	121.36	0.02	-0.11	0.07	0.66	0.2	0.1	0.5	0.5
5/16/2018	13.87	100.50	12.89	124.04	0.00	-0.20	0.05	0.49	0.0	0.2	0.4	0.4
5/23/2018	14.73	90.54	12.81	125.80	0.02	-0.18	0.07	0.71	0.1	0.2	0.5	0.6
5/30/2018	15.10	88.18	11.95	118.35	0.00	-0.16	0.03	0.35	0.0	0.2	0.3	0.3
6/6/2018	15.75	87.79	11.36	114.12	0.02	-0.34	0.05	0.55	0.1	0.4	0.4	0.5
6/13/2018	16.06	96.05	11.24	113.46	0.00	-0.13	0.08	0.87	0.0	0.1	0.7	0.8
6/20/2018	17.68	106.14	11.24	117.71	0.06	-0.08	0.09	1.32	0.3	0.1	0.8	1.1
6/26/2018	18.65	110.64			0.02	0.03			0.1	0.0		
7/3/2018	18.62	109.80	10.66	113.66	0.02	-0.07	0.05	0.55	0.1	0.1	0.5	0.5
7/11/2018	19.81	112.22	11.06	121.07	0.03	-0.11	0.13	1.61	0.1	0.1	1.1	1.3
7/17/2018	21.24	116.31			0.08	-0.65			0.4	0.6		
7/27/2018	22.14	125.13	10.24	117.04	0.06	-0.02	0.10	1.32	0.2	0.0	1.0	1.1

Table 2.1: Cast results at Camas WA, 2017-2018, with the columns in bold showing the percentage change between the surface and river bottom measurements.

Date	Water Column Average Value		Surface minus bottom		% change	
	°C	uS cm ⁻¹	°C	uS cm ⁻¹	°C	uS cm ⁻¹
11/8/2017	9.48	45.56	-0.04	-0.06	0.4	0.1
11/16/2017	9.83	47.73	0.00	-0.25	0.0	0.5
12/14/2017	5.01	45.91	-0.03	-0.07	0.7	0.2
12/22/2017	6.70	55.54	-0.08	-0.07	1.2	0.1
1/4/2018	5.88	45.25	0.00	0.20	0.1	0.4
1/11/2018	7.80	55.42	0.12	-2.05	1.5	3.8
1/18/2018	8.43	48.66	0.13	0.28	1.5	0.6
1/25/2018	7.68	46.08	0.10	-0.02	1.3	0.0
2/1/2018	8.34	42.82	0.06	0.17	0.8	0.4
2/8/2018	9.28	50.15	0.13	0.26	1.4	0.5
2/15/2018	7.32	55.50	0.13	0.89	1.8	1.6
2/22/2018	6.16	54.84	0.16	0.82	2.5	1.5
3/1/2018	6.74	55.90	0.33	0.37	4.7	0.7
3/8/2018	7.68	57.33	-0.02	0.06	0.2	0.1
3/15/2018	9.52	50.47	0.13	0.08	1.3	0.2
3/22/2018	9.13	54.97	0.08	-0.03	0.8	0.1
3/29/2018	9.24	58.06	0.41	0.93	4.2	1.6
4/8/2018	10.45	49.88	0.04	0.13	0.4	0.3
4/16/2018	9.47	46.49	0.03	-0.01	0.3	0.0
4/26/2018	13.79	59.31	0.61	0.91	4.3	1.5
5/3/2018	12.99	55.85	0.56	1.19	4.1	2.1
5/10/2018	15.90	64.58	0.26	0.20	1.6	0.3
5/17/2018	16.63	61.69	0.12	0.20	0.7	0.3
5/24/2018	17.47	63.43	0.71	0.99	3.9	1.5
5/31/2018	16.52	59.96	0.18	-0.03	1.1	0.1
6/7/2018	17.81	64.96	0.06	-0.48	0.3	0.7
6/14/2018	17.09	68.80	0.34	0.57	2.0	0.8
6/21/2018	19.62	79.01	0.17	-0.03	0.8	0.0
6/27/2018	22.17	81.58	1.14	1.77	4.9	2.1
7/5/2018	21.79	77.91	0.73	1.27	3.2	1.6
7/12/2018	21.96	82.86	0.21	0.43	1.0	0.5
7/19/2018	23.76	84.83	0.30	0.23	1.2	0.3
7/24/2018	24.32	84.20	0.07	0.10	0.3	0.1

(a)

Date	Water Column Average Value		Surface minus bottom		% change	
	°C	uS cm ⁻¹	°C	uS cm ⁻¹	°C	uS cm ⁻¹
7/19/2017	25.49	86.28	14.61	12.21	36.4	12.4

(b)

Date	Water Column Average Value		Surface minus bottom		% change	
	°C	uS cm ⁻¹	°C	uS cm ⁻¹	°C	uS cm ⁻¹
3/13/2018	6.33	91.32	0.05	-0.26	0.8	0.3

(c)

Table 2.2: (a) Cast results at Willamette Park OR, 2017-2018, with the columns in bold showing the percentage change between the surface and river bottom measurements. (b) Cast results in Ross Island Lagoon, with the columns in bold showing the percentage change between the surface and river bottom measurements. (c) Cast results in the Columbia mainstem near the Beaver Army Terminal site, 2017-2018, with the columns in bold showing the percentage change between the surface and river bottom measurements.

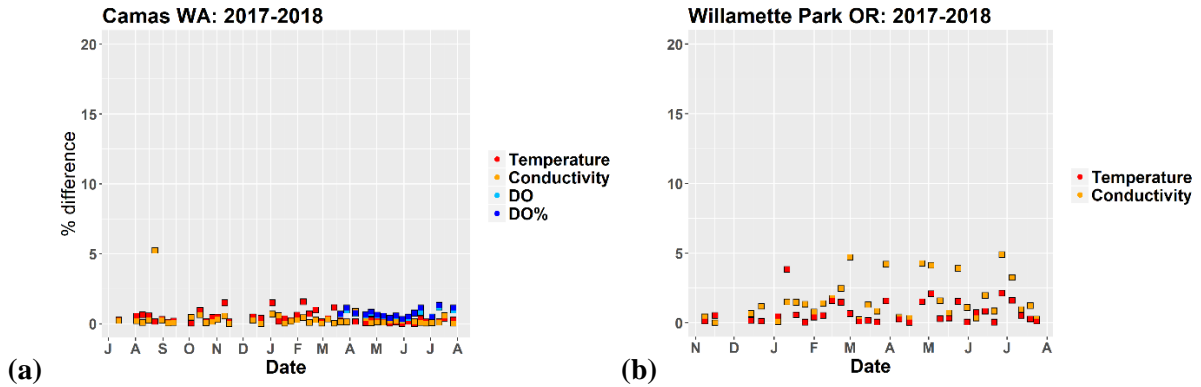


Figure 2.17: (a) Percentage difference between surface and bottom values in the Columbia for temperature, conductivity, dissolved oxygen concentration, and dissolved oxygen saturation. (b) Percentage difference between surface and bottom values in the Columbia for temperature and conductivity.

5.0 Discussion

5.1 Water column stratification

The CTD casts reveal little or no stratification in the water column in either river. Temperature in the Columbia never differed by more than 1-2% between the surface and the channel bottom (Table 2.1). The main stem of the Columbia on March 13th showed less than 1% difference between the surface and the 1% light depth, consistent with trends observed at Camas (Table 2.2c). In the Willamette, the degree of temperature stratification remained low for most weeks, with a few exceptions to the general trend of less than 2% water column variance (Table 2.2a). On the sampling dates of March 1st, March 29th, April 26th, May 3rd, May 24th, June 27th, and July 5th, peaks of 4.7%, 4.2%, 4.3%, 4.1%, 3.9%, 4.9%, and 3.2% were recorded, respectively, indicating that the Willamette may be more subject to temperature stratification than the Columbia. A possibility could be low flow and longer residence times leading to a greater degree of stratification, but these dates do not correspond with periods of low flux in the Willamette (Figure 1.2). Finding the percentage change in temperature in the diurnal cycle for each of these days showed a 5%, 9%, 8%, 3%, 3%, 2%, and 4% difference between minimum and maximum temperatures, respectively, indicating that the water column variance could be greater or less than daily

temperature variance and thus not ruling out the significance of the stratification measurement. For comparison however, in the Ross Island lagoon (Table 2.2b), which was sampled in July 2017, the surface was 36.4% warmer than the bottom, showing what would be expected in a highly stratified body of water with long residence times.

Conductivity varied by less than 1% throughout the year in the Columbia (Table 2.1), with the exception of August 23rd, 2017, at which point the surface conductivity was 5.2% greater than at the bottom. While this does correspond with a period of relatively low flow (Figure 1.2), which might feasibly lead to some degree of stratification as longer residence times would be more favorable for the formation of a halocline, the weeks immediately before and after also saw lower flow than the rest of the year, and fit the rest of the trend in conductivity which showed no stratification, making interpretation of that single week uncertain. The casts in the Columbia main stem on March 13th revealed a difference less than 1% (Table 2.2c). In the Willamette, conductivity varied by no more than about 1-2% between depths (Table 2.2a) with the exception of November 1st, where a peak of 3.8% was observed. This did not correspond with any of the observed peaks in temperature stratification, making interpretation difficult.

Dissolved oxygen concentration depth profiles of the Columbia, taken from March 21st on, varied by up to only around 1% between the surface and the bottom (Table 2.1, Figure 2.17a), as did the measurements of oxygen saturation. This indicates that while phytoplankton growth rates may be highest near the surface, the results of their activity are quickly mixed through the water column.

Regression analyses of nitrate between depths showed very little difference in either river (Figure 2.13a, b), with R^2 values of 0.9946 and 0.9969, and slopes of 1.00294 and 1.0086. However, the relationship of phosphate between depth groups was weak: even after the removal of the most extreme outliers, the regressions for the Columbia and Willamette had R^2 values of 0.3657 and 0.3826, and slopes of 0.51985 and 0.6829 (Figure 2.13c, d). These slopes implied a higher concentration of phosphate near the surface in both rivers, although the variation through time was high.

Chlorophyll samples between depths showed very little difference, tracking each other very closely throughout the year in both rivers (Figure 2.8a, b). Regression analysis between depths revealed a very little difference between groups (Figure 2.9), with an R^2 value in the Columbia of 0.9662 and slope of 0.99214, and an R^2 of 0.9042 and slope of 1.05317 in the Willamette.

Taken together, these observations are largely supportive of the mixing hypothesis, showing that rapid vertical transport of pelagic particles leads to a homogeneous water mass that can be modeled as uniform from the surface to the benthos. The Willamette does show slightly more variance between depths as shown in the CTD casts, but because this difference is small and does not appear to coincide consistently with any of the other physical parameters we measured (river discharge, temperature, turbidity), this inconsistency may be the result of other physical effects not measured here.

Despite the clearly uniform mixing of nitrate, the phosphate measurements showed only a weak relationship between depths (Figure 2.13c, d). Turnover rate of phosphate may be higher at the surface, but given the picture of a well-mixed water column implied by the majority of other measurements, we can model the overall contributions of the river systems to carbon and inorganic nutrient cycling assuming a well-mixed water column.

5.2 Light depth measurements

Light penetration in the Columbia River was consistently greater than in the Willamette, an observation reflected both in the light cast measurements (Figure 2.15) and a comparison of turbidity between the rivers (Figure 2.6c, d). The 1% light depth in the Columbia ranged from approximately 4-10 meters, with the deepest penetration depths – and thus clearest water – corresponding with the months of January and May. These minima coincided with periods of low discharge. The clearer water was likely the result of a combined lack of sediment suspension and lack of biological activity in the winter months. However, the winter as a whole fluctuated considerably, with some of the shallowest light depths recorded as well (approximately 4 meters), most likely due to an increase in particulate matter influx

during storm events. During the course of the spring phytoplankton bloom, the light depth became consistently shallow (4-6 meters) from mid-April to late June. This coincided with observed on-site phytoplankton blooming in the river as well as higher river discharge, both of which have the potential to increase the rate of light decay. The light depth dropped again as discharge decreased, returning to the 7-7.5-meter range observed in late summer through fall 2017.

In the Willamette, 1% light depths were consistently shallower than in the Columbia during the fall and winter, with the shallowest depths (approximately 2 meters) corresponding with the large peaks of turbidity (Figure 2.15c) and discharge events (Figure 1.2) seen in February, March, and April. As flow in the Willamette decreased in May through July, the water column in the Willamette became clearer, with the deepest photic zone depth at approximately 7.5 meters in mid-May. This coincided with a period of low discharge in the river, suggesting that a lack of runoff during that period led to a decrease in the amount of suspended particles in the river.

Our attenuation coefficients, from which our light depths were derived, were typically in the 0.6-1.1 range in the Columbia, while the Willamette coefficients ranged from 0.6 to 2.2. A higher coefficient indicates more rapid light decay with depth and thus more suspended particles. While this shows that the Willamette was more variable and potentially more light-limited at some parts of the year, a survey of 31 temperate rivers by Basu & Pick (1996) found a range of 0.6-5.4, with values of 1-2 being typical, suggesting that light attenuation in the Columbia and Willamette may be low compared to other rivers.

5.3 Primary production and respiration

During the period of sensor deployment, the Columbia River showed net autotrophy throughout the year (Figure 2.2a), with the exception of two points in September when it was briefly heterotrophic. A major peak in GPP of approximately $70 \mu\text{M O}_2 \text{d}^{-1}$ and corresponding NEM peak of $30 \mu\text{M O}_2 \text{d}^{-1}$ in early May, corresponding with early observations of the spring phytoplankton bloom, was followed by a drop in production, reaching a minimum GPP of around $30 \mu\text{M O}_2 \text{d}^{-1}$ and NEM of around $10 \mu\text{M O}_2 \text{d}^{-1}$ in

early June. After this, production rose again through the summer, with a maximum of over $75 \mu\text{M O}_2 \text{d}^{-1}$ in late July, although NEM did not increase as much, because ER continued to increase until late summer, with a maximum of around $60 \mu\text{M O}_2 \text{d}^{-1}$ respired. An equivalent peak in GPP and ER was observed previously in late July, 2017. Chlorophyll followed a similar pattern to production in the Columbia, with a maximum peak of $22.5 \mu\text{g L}^{-1}$ coinciding with the initial peak in GPP and NEM. However, like NEM, the second peak of chlorophyll in late July did not exceed the first. Because ER continued to rise throughout the summer, this indicates that lower discharge (Figure 1.2) leading to higher residence times, and higher water temperatures (Figure 2.6a) may have led to more heterotrophic activity, preventing the river from being as strongly autotrophic as it was in early June.

In the Willamette (Figure 2.2b), the sensor detected relatively low levels of production and respiration through most of the year ($\sim 10 \mu\text{M O}_2 \text{d}^{-1}$), and very high peaks of GPP and ER in August 2017 ($200\text{-}250 \mu\text{M O}_2 \text{d}^{-1}$) and July 2018 ($150\text{-}200 \mu\text{M O}_2 \text{d}^{-1}$). In both of these cases, ER exceeded GPP and caused the river to display net heterotrophy, indicating that aerobic bacterial growth likely exceeded phytoplankton growth. These large peaks coincided with periods of low discharge and thus presumably high residence times (Figure 1.2), and high temperatures (Figure 2.6b), conditions favoring growth of phytoplankton and bacteria. This period also closely matches the months of lower turbidity (Figure 2.6d) and deeper 1% light depths (Figure 2.15), supporting the prediction that primary production in the Willamette is light-limited during other parts of the year.

BOD incubation measurements from Camas showed a significant relationship to GPP measurements from the sensor (Figure 2.2c, 2.3), with peaks in May and July, and a local minimum in June. Likewise, in the Willamette, a sharp rise in late summer was detected (Figure 2.2d), similar to the pattern shown by the sensor. However, this rise was not nearly as high as the increase recorded by the sensor. In both cases, hourly BOD measurements of respiration from the dark bottles gave consistently low measurements as compared with *in situ* data, with as much as a tenfold difference. This means that although NEM measurements from the “light” groups may be accurate, the BOD-derived values of ER

are underestimates. This discrepancy in the Willamette may be the result of the physical distance between the sampling site (Figure 1.3c) and the SATURN-06 sensor (Figure 1.3d), which is downriver of the Ross Island lagoon and so may detect much higher rates of GPP and ER from the large annual cyanobacteria blooms observed in the lagoon.

5.4 BOD discrepancy

The unexpected result of the BOD experiments, in which measured respiration was far less than the values calculated from the sensor, requires us to eliminate some possible sources of error. The respiration rates from the sensor might appear higher due to an underestimation of the k_{wind} term (4.1), which would cause the estimated biological flux to seem larger due to some of the abiotic oxygen loss to wind diffusion inflating the number. We tested this possibility by running our ER calculations at different simulated wind speeds, as well as testing the sensitivity of the k_{wind} term at different wind speeds, finding that the effect of wind on ER estimates in both rivers was negligible at the speeds recorded during the study period (Figure 2.1). Another possibility considered was calibration drift of the DO probe, but this can be discounted as well, because the BOD rates involve measuring the DO concentration before and after incubation to infer rate of change, and so a probe that is improperly calibrated should still yield the same difference between time points, even if the values themselves have drifted. Significant oxygen contamination during measurement can be ruled out because samples were only exposed to the open air for 3-5 seconds at most, before being measured and sealed. A final possibility could be light contamination beneath the shroud that was placed over the dark bottles, leading to unwanted photosynthesis taking place. We tested this by placing a terrestrial light sensor under the shroud. It recorded a value of less than $0.5 \mu\text{mol photons m}^{-2} \text{s}^{-1}$, below the limit at which most phytoplankton can photosynthesize (Peterson et al. 1987).

To our knowledge, no previous studies have compared hourly BOD respiration with open-water estimates in the Columbia or Willamette, making this finding significant. Given the regularity of the low respiration rates encountered in the samples, it seems likely that pelagic respiration in the river mainstems

may be largely outweighed by respiration from other sources. A well-mixed, turbulent river may distribute the net effects of respiration evenly and so allow them to be detected by an open-water sensor, whereas samples represent an isolated capture of a pelagic microbial community that, once removed from *in vivo* conditions, does not display the same overall trophic dynamics. This would be the case if, for instance, most aerobic respiration in the river occurs in the benthos or at the edges of the river, or is found upstream of the sample sites. In the case of the Willamette, the sensor may see a stronger signal than the incubations because it is located downstream of the Ross Island Lagoon, which sees a massive cyanobacteria bloom in summer, whereas the sampling site is located upstream. This would result in the products of both production and respiration reaching the sensor but not the sampling bottles. This does not explain why respiration was disproportionately lower than production in the samples, however, nor why the Columbia displays the same discrepancy.

While previous investigations of the Columbia (Crump et al. 1998, 2017) and other estuaries (Hopkinson 1985, Wainwright & Hopkinson 1997) have clearly documented that the pelagic biological activity of resuspended particle-attached bacteria is significant in the ETM of the lower estuary as they respire POC, it may be that in the upper portion of the estuary mainstem and the Willamette, the majority of bacterial respiration is effected by benthic bacterial communities that feed on POC in the sediment, as has been observed in other temperate rivers (Edwards et al. 1990, Fischer & Pusch 2001). These investigations revealed far higher concentrations of bacteria in the sediment and in adhered biofilms than in the pelagic zone, and sedimentary aerobic activity up to an order of magnitude higher than in the pelagic zone. If this assumption is valid, it precludes the possibility that metazoans not captured in the samples, such as fish and invertebrates, accounts for the difference in respiration. If the rivers surveyed are representative of temperate rivers in general, then the Columbia and Willamette may be typical in this regard. While respiration may be predominantly benthic, GPP was largely similar between BOD and open-water estimates, so it is likely that primary production in both rivers is mostly pelagic.

The implications of this discrepancy are important to consider for studies which rely on whole-water surface grabs to measure water quality of the rivers. While the water columns are well-mixed, the spatial heterogeneity of microbial communities should not be underestimated.

5.5 Phytoplankton and nutrient cycling

Chlorophyll concentrations in the Columbia (Figure 2.8a) followed a similar pattern to NEM (Figure 2.2a), but the largest peak of chlorophyll at around $22.5 \mu\text{g L}^{-1}$ coincided with the initial peak of production and then dropped in early June and the second peak was not as high. Because discharge dropped precipitously in June-August (Figure 1.2) while temperatures (Figure 2.6a) and ER (Figure 2.2a) continued to rise, it is probable that POC produced by the plankton experienced longer residence times and so could be more thoroughly respired, leading to a relatively higher rate of ER and thus a lower NEM signal. Estimated phytoplankton biomass based on a C:Chl mass ratio of 25:1 showed that phytoplankton biomass and NEM track each other closely (Figure 2.10a). The river was a net exporter of organic carbon throughout the year except during September 2017, when it was briefly heterotrophic.

To show the total contribution of the river main stem to carbon cycling, we multiplied the volumetric values by daily flux, yielding the daily net change in organic carbon (Figure 2.10c). By normalizing the signal to flux, this also demonstrated that the drop in NEM in June was not only the result of higher discharge leading to dilution of particles in the river. This “dip” corresponds with one of the lowest observed points of the N:P ratio (Figure 2.11e), which remained close to the Redfield ratio for several weeks and then rose somewhat afterward. This implies that during that period, the Columbia became N-limited as reactive nitrogen was depleted from the system (Figure 2.14a). As phytoplankton activity dropped, nitrate continued to be fluxed into the river, eventually reaching a level in mid-June when phytoplankton growth could rise again, leading to the observation of the second bloom starting in July (Figure 2.2a). At this point, phytoplankton biomass and NEM remained relatively stable, with GPP increasing strongly but the lower water mass and higher temperatures fueling increased growth of aerobes that accounted for a corresponding steady rise in ER. This picture of the Columbia as an autotrophic

system contrasts with the general view of most rivers as sinks for particulate carbon imported from tributaries and runoff (Cole et al. 2007).

In the Willamette, phytoplankton biomass remained stable and relatively low ($<100 \mu\text{g L}^{-1}$) through fall, winter, and early spring (Figure 2.10b). Increases to $200\text{-}300 \mu\text{g POC L}^{-1}$ in the summer were vastly outweighed by drops in NEM to a net loss rates of $1000 \mu\text{g L}^{-1} \text{d}^{-1}$ in August 2017 and $\sim 500 \mu\text{g L}^{-1} \text{d}^{-1}$ in July 2018. Three small spikes of net autotrophy in November, January, and April corresponded with three major flux events (Figure 1.2), which are also apparent in total carbon flux estimations of the Willamette (Figure 2.10d) without subsequent increases in ER. The Willamette does not appear to be N- or P-limited during these periods (Figure 2.11f), and ER is at its lowest observed, which suggests that the high discharge rates at these points may have diluted the river and not allowed sufficient residence times for full respiration of photosynthesis-produced POC before transporting it downstream. However, because these peaks do not correspond with strong increases in phytoplankton biomass (Figure 2.10b), it is possible that the small volumetric values recorded at those points were more susceptible to error, and when multiplied by flux were dominated by the signal, showing an erroneously high value. Because the Willamette displayed such a stark contrast between summer months and the rest of the year, our description of it as a heterotrophic “brown” river should be revised. While its overall net contribution to organic carbon during the study period was negative (-236 Mg y^{-1}), this was almost entirely accounted for by the large summer bloom and subsequent rise in bacterial production, whereas a “brown” river would have low levels of photosynthesis for most of the year due to light limitation. In mid-August 2017, the high rates of production and respiration abruptly shifted from a net POC respiration rate of nearly $1000 \mu\text{g L}^{-1} \text{d}^{-1}$ to a positive rate on the order of $100 \mu\text{g L}^{-1} \text{d}^{-1}$. This decline occurred in less than a week, and coincided with a substantial spike in turbidity in the Willamette (Figure 2.6d) as well as the first rain event of the summer (NWS 2017). This indicates that while turbidity was lower during the summer and permitted the large bloom to occur, the abrupt spike in turbidity caused by the rain event led to a rapid decrease in primary production, as the high rates of phytoplankton production could no longer

be sustained, leading to a corresponding drop in bacterial respiration, as the daily supply of oxygen (Figure 2.2b) and organic carbon (Figure 2.5b) suddenly diminished.

The concentration of nitrate dropped during the increase in GPP and ER in late summer (Figure 2.14b), likely due to a combination of drawdown by plankton and also a lack of influx due to low discharge (Figure 1.2). The N:P ratio dropped to a minimum of 19:1 (Figure 2.11f), and DIN concentrations and NEM measured in organic nitrogen followed inverse patterns, suggesting that the amount of DIN was controlling NEM rates during this period, with nitrate limitation resulting in a slowing of GPP, and the subsequent replenishing of nitrate leading to another increase in NEM.

6.0 Conclusions

The validation of the water column mixing hypothesis made reliable estimates of phytoplankton primary production and the resulting nutrient and organic carbon fluxes in the Columbia and Willamette rivers possible. Evidence is strong that the rivers both have sufficient flow rates to disperse particles throughout the water column, and thus allow the byproducts of photosynthesis to be detected by a sensor installed at any depth. This allowed us to use the sensors to track the seasonal phytoplankton dynamics of both rivers and investigate the degree to which hydrological impacts of dams influence the greening of the Columbia, as well as to quantify the role both rivers play in the carbon budget.

The Columbia River displayed annual patterns of primary production and respiration consistent with the growing body of evidence that large dams contribute to the greening of the river (Weitkamp 1994, Sullivan et al. 2001, Bottom et al. 2005, Maier & Peterson 2013, Maier & Simenstad 2009). The river had a relatively deep photic zone (4-10m), and rates of primary production that peaked in early summer, maintaining an autotrophic state throughout most of the year, and exporting up to 300 Mg of particulate organic carbon per day in the reach below the Bonneville Dam during the height of the spring phytoplankton bloom in mid-May. This is consistent with the description of the Columbia as “green” river, in which phytoplankton production results in a net export of POC through the estuary and fueling

the high levels of bacterial secondary production observed in the estuarine turbidity maximum. This also means that inorganic nutrients are consumed at increased rates as the phytoplankton grow, causing them to exit the estuary and enter the Columbia River plume and coastal ocean waters in an organic form. The Willamette, by contrast, does not fully fit the description of a heterotrophic “brown” river. While it displayed very low biological activity throughout the year, it was slightly autotrophic during most of that period, and while it was a net sink of organic carbon during the summer bloom, this heterotrophic period also showed high rates of primary production, which would not be expected in a “brown” river. This is most likely the result of light limitation between fall and spring, and a combination of clearer water and longer residence times in the summer. As a result, during most of the year, inorganic nutrients largely pass through the Willamette and enter the Columbia unchanged, but biological activity causes a drawdown in summer. It is generally accepted that absent the primary production provided in dam-controlled reservoirs like the Columbia, most rivers are heterotrophic, and net sources of CO₂ (Butman & Raymond 2011), but while this is true for the Willamette, it may not fit the “brown” model for substantial periods during the year.

The consistent discrepancy in hourly respiration estimates between sensor and BOD data shows that some difference exists between rates of respiration across the whole river system and pelagic rates. While the cause of the difference in measurements is still unknown, it might be determined by further BOD experiments that record changes in dissolved oxygen at a higher temporal resolution, and by incubation of sediment cores from the rivers to determine the relative contribution of benthic microbes to respiration in the system.

7.0 References

Alin, S., Siedlecki, S., Hales, B., Mathis, J., Evans, W., Stukel, M., Gaxiola-Castro, G., Hernandez-Ayon, J.M., Juranek, L., Goñi, M., Turi, G., Needoba, J., Mayorga, E., Lachkar, Z., Gruber, N., Hartmann, J., Moosdorf, N., Feely, R., & Chavez, F. (2012). Coastal carbon synthesis for the continental shelf of the North American Pacific Coast (NAPC): Preliminary results. *Ocean Carbon and Biogeochemistry News*, **5**(1), 1-5.

APHA, AWWA, & WEF (1992). Standard methods for examination of water and wastewater, 18th edition. Washington D.C., USA: American Public Health Association.

Apple, J.K., Del Giorgio, P.A., & Kemp, W.M. (2006). Temperature regulation of bacterial production, respiration, and growth efficiency in a temperate salt-marsh estuary. *Aquatic Microbial Ecology*, **43**, 243-254.

Armstrong, F.A., Stearns, C.R., & Strickland, J.D. (1967). The measurement of upwelling and subsequent biological processes by means of the Technicon Autoanalyzer[®] and associated equipment. *Deep Sea Research*, **14**, 381-389.

Basu, B.K., & Pick, F.R. (1996). Factors regulating phytoplankton and zooplankton biomass in temperate rivers. *Limnology and Oceanography*, **41**(7), 1572-1577.

Bottom, D.L., Simenstad, C.A., Burke, J., Baptista, A.M., Jay, D.A., Jones, K.K., Casillas, E., & Schiewe, M.H. (2005). Salmon at river's end: the role of the estuary in the decline and recovery of Columbia River salmon. *NOAA Technical Memorandum NMFS-NWFSC-68*.

Bureau of Planning and Sustainability (2010). Willamette river dredged material management plan project. City of Portland. Retrieved from <https://www.portlandoregon.gov/bps/article/145503>

Butman, D., & Raymond, P.A. (2011). Significant efflux of carbon dioxide from streams and rivers in the United States. *Nature Geoscience*, **4**, 839-842.

Caffrey, J.M. (2003). Production, respiration and net ecosystem metabolism in U.S. estuaries. *Coastal Monitoring through Partnerships: Proceedings of the Fifth Symposium on the Environmental Monitoring and Assessment Program (EMAP)* Pensacola Beach, FL, U.S.A., April 24-27, 2001, 207-219.

Cole, J.J., Prairie, Y.T., Caraco, N.F., McDowell, W.H., Tranvik, L.J., Striegl, R.G., Duarte, C.M., Kortelainen, P., Downing, J.A., Middelburg, J.J., & Melack, J. (2007). Plumbing the global carbon cycle: Integrating inland waters into the terrestrial carbon budget. *Ecosystems*, **10**, 171-184.

Delzer, G.C., & McKenzie, S.W. (2003). Five-day biochemical oxygen demand. *United States Geological Survey Techniques of Water-Resources Investigations Report, Book 9-A7(3)*, 1-21.

Donner, S.D., & Scavia, D. (2007). How climate controls the flux of nitrogen by the Mississippi River and the development of hypoxia in the Gulf of Mexico. *Limnology and Oceanography*, **52(2)**, 856-861.

Edwards, R.T., Meyer, J.L., & Findlay, S.E.G. (1990). The relative contribution of benthic and suspended bacteria to system biomass, production, and metabolism in a low-gradient blackwater river. *Journal of the North American Benthological Society*, **9(3)**, 216-228.

Falkowski, P., Scholes, R.J., Boyle, E., Canadell, J., Canfield, D., Elser, J., Gruber, N., & Hibbard, K. (2000). The global carbon cycle: A test of our knowledge of Earth as a system. *Aquatic Microbial Ecology*, **43(3)**, 243-254.

Field, C., Behrenfeld, M., & Randerson, J. (1998). Primary production of the biosphere: Integrating terrestrial and oceanic components. *Science*, **281**, 237-241

Fischer, H., & Pusch, M (2001). Comparison of bacterial production in sediments, epiphyton and the pelagic zone of a lowland river. *Freshwater Biology*, **46**, 1335-1348.

Gilbert, M., Needoba J., Koch, C., Barnard, A., & Baptista, A. (2013). Nutrient loading and transformations in the Columbia River Estuary determined by high-resolution in situ sensors. *Estuaries and Coasts*, **36(4)**, 708–727.

Holmes, R. M., Aminot, A., K erouel, R., Hooker, B. A., & Peterson, B. J. (1999). A simple and precise method for measuring ammonium in marine and freshwater ecosystems. *Canadian Journal of Fisheries and Aquatic Sciences*, **56(10)**, 1801-1808.

Hopkinson, C.S., Jr. (1985). Shallow-water benthic and pelagic metabolism: Evidence of heterotrophy in the nearshore Georgia Bight. *Marine Biology*, **32(530)**, 19-32.

Howarth, R., Chan, F., Conley, D.J., Garnier, J., Doney, S.C., Marino, R., & Billen, G. (2011). Coupled biogeochemical cycles: Eutrophication and hypoxia in temperate estuaries and coastal marine ecosystems. *Frontiers in Ecology and the Environment*, **9**(1), 18-26.

Kinsey, J.D., Corradino, G., Ziervogel, K., Schnetzer, A., & Osburn, C.L. (2018). Formation of chromophoric dissolved organic matter by bacterial degradation of phytoplankton-derived aggregates. *Frontiers in Marine Science*, **4**(430), 1-16.

Maier, M.A., & Peterson, T.D. (2014). Observations of a diatom chytrid parasite in the lower Columbia River. *Northwest Science*, **88**(3), 234-245.

Maier, G., & Simenstad, C. (2009). The role of marsh-derived macrodetritus to the food webs of juvenile chinook salmon in a large altered estuary. *Estuaries and Coasts*, **32**(5), 984-998.

Needoba, J., Peterson, T., & Johnson, K. (2012). Method for the quantification of aquatic primary production and net ecosystem metabolism using in situ dissolved oxygen sensors. In Needoba, J., Peterson, T., Johnson, K., & Tiquia-Arashiro, S. (Eds.), *Molecular Biological Technologies for Ocean Sensing*. Totowa, NJ: Humana Press.

Nelson, D. (n.d.) Save the plankton, breathe freely. *National Geographic Society*. Retrieved from <https://www.nationalgeographic.org/activity/save-the-plankton-breathe-freely/>

NOAA National Weather Service, Portland Weather Forecast Office. Retrieved from: <http://w2.weather.gov/climate/index.php?wfo=PQR>

Pauly, D., & Christensen, V. (1995). Primary production required to sustain global fisheries. *Nature*, **374**, 255-257.

Peterson, D.H., Perry, M.J., Bencal, K.E., & Talbot, M.C. (1987). Phytoplankton productivity in relation to light intensity: A simple equation. *Estuarine, Coastal and Shelf Science* **24**, 813-832.

Staeher, P., Bade, D., Koch, G., Williamson, C., Hanson, P., Cole, J., & Kratz, T. (2010). Lake metabolism and the diel oxygen technique: state of the science. *Limnology and Oceanography: Methods*, **8**, 628-644.

Sullivan, B.E., Prahl, F.G., Small, L.F., & Covert, P.A. (2001). Seasonality of phytoplankton production in the Columbia River: A natural or anthropogenic pattern? *Geochimica et Cosmochimica Acta*, **65**(7), 1125-1139.

Tranvik, L.J. (1992). Allochthonous dissolved organic matter as an energy source for pelagic bacteria and the concept of the microbial loop. *Hydrobiologia*, **229**, 107-114.

Wainwright, S.C., & Hopkinson, C.S., Jr. (1997). Effects of sediment resuspension on organic matter processing in coastal environments: A simulation model. *Journal of Marine Systems*, **11**, 353-368.

Wanninkhof, R. (1992). Relationship between wind speed and gas exchange over the ocean. *Journal of Geophysical Research*, **97**(C5), 7373-7382.

Weitkamp, L.A. (1994). A review of the effects of dams on the Columbia River estuarine environment, with special reference to salmonids. *Report to Bonneville Power Administration, Contract 227 DE_A179-93BP99021*.

Welschmeyer, N.A. (1994). Fluorometric analysis of chlorophyll *a* in the presence of chlorophyll *b* and pheopigments. *Limnology and Oceanography*, **39**(8), 1985-1992.

CHAPTER 3

Conclusions and Future Directions

1.0 Conclusions

The preceding chapters have explored the physical and biochemical principles that underlie phytoplankton primary production, and applied this knowledge to characterize the trophic dynamics of the Columbia and Willamette rivers. Phytoplankton play a crucial role in oxygen production, nutrient cycling, CO₂ uptake, and the associated production of particulate organic carbon, which supports the world's aquatic food webs. In ecosystems, they function as a means to make photochemical energy available to consumers by harnessing photons and using them to power the formation of glucose molecules. This process consumes inorganic nutrients and CO₂, and produces O₂ as a byproduct. Aerobic respiration acts in reverse, consuming organic molecules and O₂, and producing CO₂. Together, the net result of these two processes defines the trophic state of an aquatic ecosystem. Knowing this value reveals the degree to which an ecosystem is acting as a source or sink of O₂, CO₂, inorganic nutrients, and organic carbon.

The trophic states of rivers are less well documented than those of oceans and lakes. This thesis outlined the means by which the trophic states of rivers can be studied, and applied those techniques to the Columbia and Willamette rivers. A central question was the extent to which vertical mixing is present in the water columns of the rivers, because estimations of primary production and respiration that rely on data from *in situ* sensors at fixed depths are based on the assumption that measurements made at that depth are representative of the whole water column. Empirically testing that assumption revealed that it is valid: depth profile measurements showed a thoroughly homogeneous water column in both rivers, thus ensuring confidence in the accuracy of models derived from sensor data.

Primary production and respiration were measured in both rivers from July 2017 to July 2018, revealing that the Columbia River was strongly autotrophic for most of the year and thus a net source of particulate organic carbon. The Willamette had low production and respiration through fall and winter, and became strongly heterotrophic in the summer, as a large increase in primary production was matched and exceeded by a peak of respiration. These observations provide support for the view that the Columbia experiences phytoplankton blooms analogous to those seen in temperate lakes as a result of hydroelectric dams. The artificial catchment areas formed by these dams act to increase water residence times and contribute to the settlement and trapping of silt, making light more available for photosynthesis. The Willamette has no major artificial impoundments, and so water column light availability is more limited as was observed in this study through most of the year. Patterns in nutrient uptake indicate that the Columbia became N-limited in mid-summer after a long period of nitrate drawdown. The Willamette showed signs of N-limitation in the summer, but during the rest of the year dissolved nitrate concentrations were far higher than phytoplankton biomass, showing that during most of the year phytoplankton growth was far too low to significantly impact nitrate concentrations.

The different rates of hourly respiration between sensors and BOD bottles was a significant finding, and likely the result of a difference between pelagic respiration rates and whole system rates. This points to large sources of respiration and heterotrophic production occurring elsewhere, whether upriver, in side channels, or benthic microbial communities.

2.0 Future Directions

This thesis is intended to be a contribution to a growing body of literature exploring the activities of phytoplankton in rivers. Much still remains to be determined. A future study of primary production in the Columbia might include light depth measurements and BOD bottle experiments above the Bonneville Dam, to more conclusively show the effects of silt trapping on photosynthetic activity. Additionally, tracking the influence of the Willamette River as it fluxes inorganic nutrients into the Columbia would be

necessary to determine to what extent those nutrients might cause a secondary phytoplankton bloom downstream of the confluence.

A set of studies on the rates of metabolism of dissolved organic matter in whole water dark samples with more timepoints and direct measurements of carbon would allow determination of the cause of the mismatched respiration measurements, as well as incubation experiments on benthic cores from the rivers to determine whether aerobic microbes in the sediment contribute a significant fraction of the total ecosystem respiration.

Multiple years of sampling would yield a more complete picture of regular seasonal trends in primary production, nutrient fluxing, and light limitation, and give a broader perspective on what aspects of the whole system are likely to experience long term changes.